



## Short-term effects of agriculture on air pollution and climate in California

Mark Z. Jacobson<sup>1</sup>

Received 30 June 2008; revised 8 September 2008; accepted 29 September 2008; published 9 December 2008.

[1] This paper discusses the short-term effects of irrigation and albedo differences due to agriculture on California and Los Angeles air pollution and climate. High-resolution irrigation, land use, soil, albedo, and emission data were applied at the subgrid scale in the nested global-through-urban GATOR-GCMOM model to examine these issues following a comparison of baseline model results with data. In August, irrigation alone was found to increase soil moisture, thereby increasing nighttime but decreasing daytime ground temperatures more, causing a net ground cooling in California and Los Angeles. Agriculture was calculated to increase the albedo of the northern Central Valley but decrease that of the southern valley more relative to nonagricultural land today, offsetting part of the cooling due to irrigation alone. The spatial maximum day-night average August cooling in the Central Valley due to irrigation plus albedo differences from agriculture was 0.9 K at 30 m height and 2.3 K at the ground, in range of an historic 0.74–2.4 K cooling at 2 m attributed to heavily irrigated agriculture in an independent data study. When averaged over all model cells containing >0% irrigation, irrigation alone and irrigation plus albedo differences decreased day-night average 2-m temperatures by 0.44 K and 0.16 K, respectively, indicating greater local than regional effects of agriculture. In the Central Valley, irrigation increased the relative humidity, cloud water, and precipitation, shifting aerosol and soluble gas mass to clouds and rain. In the valley and Los Angeles, agriculture stabilized air, decreasing wind speeds and turbulence, increasing pollution in the absence of rain. Thus, when enhancing clouds and precipitation, agriculture decreased pollution; otherwise, agriculture increased pollution. Agriculture in parts of the polluted eastern Los Angeles basin increased fine particulate matter by ~2% and ozone by ~0.1%. All results were robust to a change in the simulation date, although further evaluation is needed to better quantify effects of agriculture on climate and air quality.

**Citation:** Jacobson, M. Z. (2008), Short-term effects of agriculture on air pollution and climate in California, *J. Geophys. Res.*, *113*, D23101, doi:10.1029/2008JD010689.

### 1. Introduction

[2] Observed global warming to date (approximately 0.75–0.85 K since 1850) is attributable primarily to warming by greenhouse gases and absorbing aerosol particles offset by cooling due to reflective aerosol particles. Regional changes in temperature, though, are also influenced by land use changes. For example, the replacement of virgin landscape with agriculture affects soil and water vapor through irrigation, albedo differences, carbon storage in land, and emissions of climate- and air-pollution-relevant gases and particles. Such emissions occur during the production and use of fertilizers and during cultivation, harvesting, and transport of agricultural food products. In this paper, agriculture's

effects on regional climate and air quality, through its impact on irrigation and albedo differences, are examined with a high-resolution nested model and data.

[3] Irrigation affects soil moisture, which affects ground temperatures, vertical temperature profiles, and evaporation. Temperature profiles affect boundary layer depths, turbulence, and winds. Evaporation affects the relative humidity, cloud formation, and precipitation. The effects of soil moisture on boundary layer circulation and/or clouds have been studied by *Zhang and Anthes* [1982], *Ookouchi et al.* [1984], *Mahfouf et al.* [1987], *Lanici et al.* [1987], *Cuenca et al.* [1996], *Emori* [1998], *Jacobson* [1999], *Fennessy and Shukla* [1999], and *Martilli* [2002], among others. *Barnston and Schickedanz* [1984] concluded from data that irrigation from 1931 to 1970 over the southern U.S. Great Plains was correlated with temperature decreases and precipitation increases. *Segal et al.* [1998] modeled a North-America-averaged rainfall increase due to irrigation over the last 100 years. *Moore and Rojstaczer* [2001], however, suggested through data analysis that irrigation-induced rainfall

<sup>1</sup>Department of Civil and Environmental Engineering, Stanford University, Stanford, California, USA.

over the Great Plains between 1950 and 1997 was minor compared with natural factors affecting rainfall.

[4] Through data analysis, *Christy et al.* [2005] suggested that temperatures in California's Central Valley increased  $0.07^{\circ}\text{C}$  per decade whereas those in the Sierra Nevada Mountains decreased  $-0.02^{\circ}\text{C}$  per decade from 1910 to 2003. They attributed the difference to an albedo decrease in the valley relative to the mountains caused by greener vegetation in the valley from increased irrigation. Conversely, *Bonfils and Lobell* [2007] estimated from data that, for 75% irrigated agricultural land in the Central Valley, summer day-night average 2-m temperatures may have decreased by  $0.7\text{--}2.4\text{ K}$ . *Kueppers et al.* [2007b, 2007a], who compared results from four regional climate models applied to the western United States, also found that irrigation combined with landcover change decreased surface temperature, as did *Adegoke et al.* [2003, 2007] and *Lobell et al.* [2006], who examined other locations.

[5] With respect to air pollution, *Jacobson* [1999] examined the effect of soil moisture on temperatures, particles and gases in Los Angeles. The study did not consider feedbacks of soil moisture to clouds and precipitation. Over a two-day period, high soil moisture resulted in thinner boundary layer depths, increasing average near-surface primary pollutant concentrations. Low soil moisture thickened boundary layer depths, decreasing concentrations. No study to date, though, has examined the effects of agriculture specifically, through irrigation or albedo differences, on air pollution.

[6] Here, the effects of irrigation and albedo differences due to agriculture on California and Los Angeles climate and air quality are examined, accounting for feedbacks to clouds and precipitation. This study differs from previous studies of the effects of agriculture in that it uses a high-resolution in space and time irrigation data set, treats subgrid application of irrigation to different soil types, and treats the physical evolution of clouds and precipitation from aerosol particles. Although Los Angeles does not have significant agricultural irrigation (as opposed to garden irrigation, which is not considered here), agricultural irrigation occurs in the eastern basin, where air pollution is highest, and this study provides an opportunity to examine the impacts of irrigation there.

## 2. Description of the Model

[7] The model used was GATOR-GCMOM, a one-way-nested global-through-urban scale Gas, Aerosol, Transport, Radiation, General Circulation, Mesoscale, and Ocean Model. The model has been evaluated against paired-in-time-and-space gas, aerosol, radiative, meteorological, and cloud data without data assimilation or spin-up in California and Los Angeles [*Jacobson*, 1997, 1999, 2001a, 2001b; *Jacobson and Kaufman*, 2006; *Jacobson et al.*, 2007]. More comparisons are shown here.

[8] Three nested domains were used: global ( $4^{\circ}\text{-SN} \times 5^{\circ}\text{-WE}$  resolution), California ( $0.2^{\circ} \times 0.15^{\circ} \approx 21.5\text{ km} \times 14.0\text{ km}$ ) and South Coast Air Basin (SCAB) ( $0.045^{\circ} \times 0.05^{\circ} \approx 4.7\text{ km} \times 5\text{ km}$ ). The global domain included 47 sigma-pressure layers up to  $0.219\text{ hPa}$  ( $\approx 60\text{ km}$ ). The regional domains included 35 layers up to  $55.3\text{ hPa}$  ( $\approx 20\text{ km}$ ), each matching the bottom 35 global-model

layers exactly. All domains included six layers in the bottom 1 km. Processes were treated the same way in all nested domains, except that the dynamical and cloud treatments differed between the global and regional domains.

[9] The model treated time-dependent dynamical, gas, aerosol, cloud, radiative, ocean, and land-surface processes. Treatment of these processes is described in detail by *Jacobson et al.* [2007], thus only some processes are discussed here. Gas photochemistry among 143 gases, 282 kinetic reactions, and 36 photolysis reactions was solved with SMVGEAR II. Aerosol processes were treated over one size distribution consisting of 12 size bins  $0.002\text{--}50\text{ }\mu\text{m}$  in diameter, and 16 aerosol components per bin (Table 1). Particle number concentration and mole concentrations of several chemicals were predicted in each bin (Table 1). Discrete size-resolved aerosol processes included emissions, binary and ternary homogeneous nucleation, condensation, dissolution, internal-particle chemical equilibrium, aerosol-aerosol coagulation, aerosol-hydrometeor coagulation, sedimentation, dry deposition, and transport [*Jacobson*, 2002, 2003].

[10] In regional domains, size- and composition-resolved aerosol-cloud interactions, cloud thermodynamics, and cloud microphysics were treated explicitly, with clouds and aerosols evolving and moving in 3-D over time [*Jacobson et al.*, 2007]. Three hydrometeor size distributions—liquid, ice, and graupel—evolved from the aerosol distribution. Table 1 shows that each of the 12 size bins ( $0.5\text{ }\mu\text{m}\text{--}8\text{ mm}$  diameter) treated in each hydrometeor distribution contained all the aerosol components in the aerosol particles they formed from. Cloud microphysical processes among all size bins included condensation, deposition, hydrometeor-hydrometeor coagulation (liquid-liquid, liquid-ice, liquid-graupel, ice-ice, ice-graupel, and graupel-graupel), aerosol-hydrometeor coagulation, liquid drop breakup, settling, evaporative cooling during drop settling, evaporative freezing (freezing during drop cooling), heterogeneous-homogeneous freezing, contact freezing, melting, evaporation, sublimation, release of aerosol cores upon evaporation/sublimation, coagulation of hydrometeors with interstitial aerosol particles, irreversible aqueous chemistry, gas washout, and lightning generation [*Jacobson*, 2003].

[11] The model treated 86 wavelengths for photolysis and 694 wavelength/probability intervals (318 UV, visible, solar-IR and 376 thermal-IR) for radiative heating. Such calculations accounted for spectral optical properties of gases, size/composition-resolved aerosols, and size/composition-resolved clouds.

### 2.1. Agricultural Land and Other Surfaces

[12] The model treated ground temperatures and moisture over subgrid surfaces (12 soil classes and roads, roofs, and water in each grid cell). It also treated vegetation over soil, snow over bare soil, snow over vegetation over soil, sea-ice over water, and snow over sea-ice over water [*Jacobson*, 2001a]. For soil surfaces, subsurface temperatures and liquid water content were calculated over time with a 10-layer subsurface module. For ocean water, the model predicted ocean mixed-layer depths, velocities, temperatures, energy transport, and mass transport over time with a 2-D ocean module that conserved potential enstrophy [*Ketefian and Jacobson*, 2009]. Nine layers existed below each ocean

**Table 1.** Aerosol and Hydrometeor Size Distributions Treated in the Model and the Chemical Constituents Present in Each Size Bin of Each Size Distribution<sup>a</sup>

Aerosol Internally Mixed	Cloud/Precipitation Liquid	Cloud/Precipitation Ice	Cloud/Precipitation Graupel
Number	Number	Number	Number
BC	BC	BC	BC
POM	POM	POM	POM
SOM	SOM	SOM	SOM
H <sub>2</sub> O(aq)-hydrated	H <sub>2</sub> O(aq)-hydrated	H <sub>2</sub> O(aq)-hydrated	H <sub>2</sub> O(aq)-hydrated
H <sub>2</sub> SO <sub>4</sub> (aq)			
HSO <sub>4</sub> <sup>-</sup>	HSO <sub>4</sub> <sup>-</sup>	HSO <sub>4</sub> <sup>-</sup>	HSO <sub>4</sub> <sup>-</sup>
SO <sub>4</sub> <sup>2-</sup>	SO <sub>4</sub> <sup>2-</sup>	SO <sub>4</sub> <sup>2-</sup>	SO <sub>4</sub> <sup>2-</sup>
NO <sub>3</sub> <sup>-</sup>	NO <sub>3</sub> <sup>-</sup>	NO <sub>3</sub> <sup>-</sup>	NO <sub>3</sub> <sup>-</sup>
Cl <sup>-</sup>	Cl <sup>-</sup>	Cl <sup>-</sup>	Cl <sup>-</sup>
H <sup>+</sup>	H <sup>+</sup>	H <sup>+</sup>	H <sup>+</sup>
NH <sub>4</sub> <sup>+</sup>	NH <sub>4</sub> <sup>+</sup>	NH <sub>4</sub> <sup>+</sup>	NH <sub>4</sub> <sup>+</sup>
NH <sub>4</sub> NO <sub>3</sub> (s)			
(NH <sub>4</sub> ) <sub>2</sub> SO <sub>4</sub> (s)			
Na <sup>+</sup> (K <sup>+</sup> , Mg <sup>2+</sup> , Ca <sup>2+</sup> )	Na <sup>+</sup> (K <sup>+</sup> , Mg <sup>2+</sup> , Ca <sup>2+</sup> )	Na <sup>+</sup> (K <sup>+</sup> , Mg <sup>2+</sup> , Ca <sup>2+</sup> )	Na <sup>+</sup> (K <sup>+</sup> , Mg <sup>2+</sup> , Ca <sup>2+</sup> )
Soil dust	Soil dust	Soil dust	Soil dust
Pollen/spores/bact.	Pollen/spores/bact.	Pollen/spores/bact.	Pollen/spores/bact.
	H <sub>2</sub> O(aq)-condensed	H <sub>2</sub> O(s)	H <sub>2</sub> O(s)

<sup>a</sup>POM is primary organic matter; SOM is secondary organic matter. H<sub>2</sub>O(aq)-hydrated is liquid water hydrated to electrolytes in solution. H<sub>2</sub>O(aq)-condensed is condensed water. Condensed and hydrated water existed in the same particles. If condensed water evaporated, hydrated water and other aerosol material remained. H<sub>2</sub>O(s) was liquid water that froze or water vapor deposited as ice. Emitted particles included fossil-fuel soot (BC, POM, H<sub>2</sub>SO<sub>4</sub>(aq), HSO<sub>4</sub><sup>-</sup>, SO<sub>4</sub><sup>2-</sup>), sea spray (H<sub>2</sub>O, Na<sup>+</sup>, K<sup>+</sup>, Mg<sup>2+</sup>, Ca<sup>2+</sup>, Cl<sup>-</sup>, NO<sub>3</sub><sup>-</sup>, H<sub>2</sub>SO<sub>4</sub>(aq), HSO<sub>4</sub><sup>-</sup>, and SO<sub>4</sub><sup>2-</sup>), biomass and biofuel burning (same chemicals as sea spray plus BC, POM), soil dust, pollen, spores, and bacteria. For sea spray and biomass/biofuel burning, K<sup>+</sup>, Mg<sup>2+</sup>, Ca<sup>2+</sup> were treated as equivalent Na<sup>+</sup>. Homogeneously nucleated species (H<sub>2</sub>O, H<sub>2</sub>SO<sub>4</sub>(aq), HSO<sub>4</sub><sup>-</sup>, SO<sub>4</sub><sup>2-</sup>, NH<sub>4</sub><sup>+</sup>) entered the internally mixed (IM) aerosol distribution. Condensing gases on the IM aerosol distribution included H<sub>2</sub>SO<sub>4</sub> and SOM. Dissolving gases in the IM aerosol distribution included HNO<sub>3</sub>, HCl, and NH<sub>3</sub>. All gases dissolved in liquid hydrometeor particles according to their effective Henry's constant. All distributions were affected by self-coagulation and heterocoagulation to other distributions.

mixed-layer grid cell to treat energy and chemical diffusion from the mixed layer to the deep ocean and ocean chemistry. Ocean and sea ice top temperatures were also affected by radiative, sensible, and latent heat fluxes [Jacobson, 2001a].

[13] Initial topsoil moisture in all model domains was interpolated spatially to each model grid cell and in time between July and August to 1 August, from 0.5-degree- and monthly resolved global reanalysis fields from *Fan and van den Dool* [2004]. Initial topsoil moisture was assumed to be the same for all subgrid soil classes in each cell, but limited by the field capacity of the soil type. Initial deep soil moisture (down to 10.2 m) in each layer of the 10-layer soil module (with layer thicknesses of 0.005, 0.01, 0.01, 0.01, 0.015, 0.025, 0.05, 0.1, 5, and 5 m, respectively) within each soil class of each cell was scaled with depth between topsoil moisture and saturation soil moisture for the soil class, in the bottom layer. The bottom layer was assumed to define the initial water table. Over time, though, the water table depth could increase if deep soil above the bottom layer became saturated.

[14] Leaf-area index varied monthly and was interpolated in time for each subgrid soil class from 1-km resolution satellite data [USGS, 2008a]. Fractional vegetation cover data used were at 1-km resolution [Zeng *et al.*, 2000]. For each of the 12 subgrid soil classes in each grid cell, it was necessary to obtain the fractional area of the soil class that contained agriculture so that irrigation could be applied proportionally to that fractional area. This fraction was determined from land use data at 1-km resolution [USGS, 1999]. The land use data set consisted of 24 land use categories, one assigned to each square kilometer. Five categories of data included agricultural land: dryland cropland and pasture, irrigated cropland and pasture, mixed

dryland/irrigated cropland and pasture, cropland/grassland mosaic, and cropland/woodland mosaic. The soil type [Miller and White, 1998] and the land use type were at 1 km resolution. As such, it was possible to determine the fractional agricultural land over each soil type in each model grid cell. Previous studies have not modeled the effect of irrigation or agriculture while treating agriculture, irrigation, and albedo at the subgrid scale.

[15] Figure 1a shows the fractional agricultural land in each grid cell, which is the product of the agricultural fraction of each soil type and the fractional area in a grid cell of the soil type, summed over all soil types. The largest fraction in the domain is 90%, and most fractions in agricultural areas are 50–80%. The figure shows a strong agricultural presence in the Central Valley and a lesser presence throughout much of the rest of California. About 3.81% of all the land area in the California domain (which included California and parts of Nevada) and 1.0% of land in the Los Angeles domain consisted of a USGS agriculture land use category.

## 2.2. Irrigation

[16] Irrigation estimates were obtained from *Salas et al.* [2006], who applied a denitrification/decomposition/embedded crop model to determine agronomic demand and an irrigation efficiency factor to account for overirrigation and irrigation efficiency in California. Irrigation estimates were at 5-km and daily temporal resolutions for 1983, 1996, and 1997. Separate data sets were available for each year assuming either 1950s or early 2000s climate conditions. Here, the 1997 data set with early 2000s climate conditions was used. The 5-km resolution data were converted to coarser model-resolution data in a water-conserving manner for each day of the year. Figure 1b shows an example of the

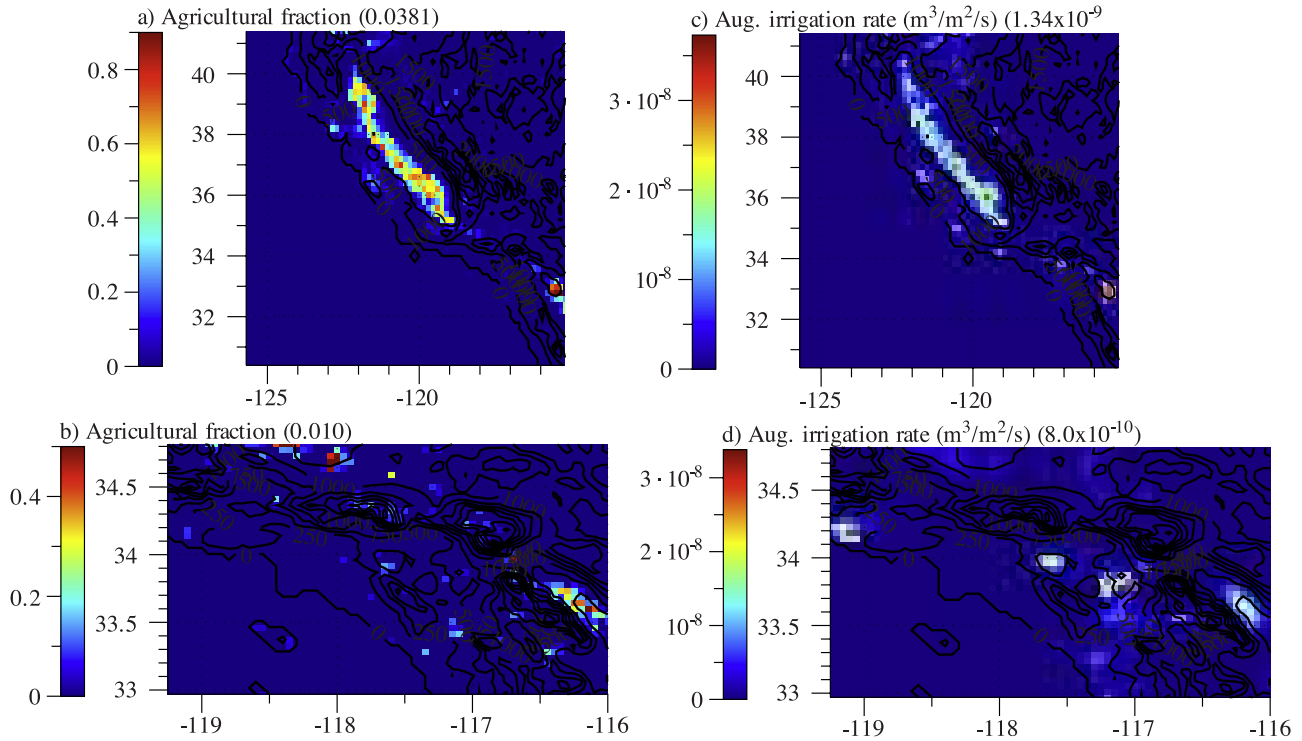


**Figure 1.** Fraction of land as agriculture [USGS, 1999] and August-averaged irrigation rate [Salas *et al.*, 2006] in the California and SCAB (Los Angeles) domains. The number in parentheses is the average over all land points in the figure. Contours are topography.

resulting irrigation rates averaged over August. The figure shows that most irrigation in California occurred in the Central Valley. Some irrigation occurred to the east and northeast of San Diego ( $33^{\circ}\text{N}$ ) and in the eastern Los Angeles basin ( $117^{\circ}\text{W}$ ,  $34^{\circ}\text{N}$ ). Salas *et al.* [2006] conclude that the daily irrigation rate varied significantly, decreasing, for example, from about  $7000$  to  $2500$   $\text{m}^3/\text{d}$  from 1 to 31 August in San Joaquin County.

[17] Daily irrigation, which was now a model grid cell-average value, was applied proportionally in each grid cell to the fraction of agricultural land in each subgrid soil class in the grid cell. Thus, for example, if a grid cell consisted of 50% sandy loam and 50% clay loam, and the agriculture fraction of sandy loam was 30% and that of clay loam was 60%, one third of all irrigation in the cell was applied to the sandy loam soil class and two-thirds was applied to the clay loam class. In the California domain, about 24.09% of all grid cells by number (or 23.75% of the total domain by area) contained agriculture, but the grid cells with any agriculture contained, on average, only 8.213% agricultural land (with peaks of 50–90% in the Central Valley; Figure 1a), according to USGS land use classification.

[18] The August irrigation rate over actual agricultural land ( $44,370$   $\text{km}^2$ ) was  $1.82 \times 10^{-8}$   $\text{m}^3/\text{m}^2/\text{s}$ ; that over all grid cells in the California model domain containing any agriculture was  $2.87 \times 10^{-9}$   $\text{m}^3/\text{m}^2/\text{s}$ ; and that averaged over all land in the model domain was  $1.34 \times 10^{-9}$   $\text{m}^3/\text{m}^2/\text{s}$ . Multiplying any of these numbers through by its respective land area gives a total August irrigation rate in California in all cases of 2.18 billion  $\text{m}^3/\text{August}$  [Salas *et al.*, 2006], approximately 14.2% of California’s annual average irrigation rate.

### 2.3. Albedo

[19] Contemporary surface albedo data were obtained from  $0.05^{\circ}$  resolution satellite data in seven spectral bands ( $0.47$ ,  $0.55$ ,  $0.65$ ,  $0.86$ ,  $1.24$ ,  $1.63$ , and  $2.11$   $\mu\text{m}$ ) [USGS, 2008b]. These observed current albedos were interpolated in real space to the resolution of each model grid cell and in wavelength space to each of the 318 model solar spectral wavelengths/probability intervals. Since each model grid cell was divided into multiple soil classes, this current “observed” albedo over the grid cell equaled

$$A_{cur} = \sum_i f_{s,i} [A_{non-ag,i} (1 - f_{ag,i}) + A_{ag} f_{ag,i}] \quad (1)$$

where  $f_{s,i}$  is the fraction of the cell occupied by soil class  $i$ ,  $A_{non-ag,i}$  is the albedo of land without agriculture in the soil class,  $A_{ag}$  is the albedo of agricultural land (assumed independent of soil class here), and  $f_{ag,i}$  is the fraction of land occupied by agriculture in the soil class. Since the current albedo was known only to the grid scale, it was assumed to be constant across the grid cell. As such, the equation for the current albedo for a soil class is  $A_{cur} = A_{non-ag,i} (1 - f_{ag,i}) + A_{ag} f_{ag,i}$ . From this equation, the fraction of land not currently occupied by agriculture in a soil class is exactly

$$A_{non-ag,i} = \frac{A_{cur,i} - A_{ag} f_{ag,i}}{1 - f_{ag,i}} \quad (2)$$

Equation (2) was solved for each soil class in each grid cell and wavelength since the soil class fraction and the agricultural fraction of each soil class in each cell were

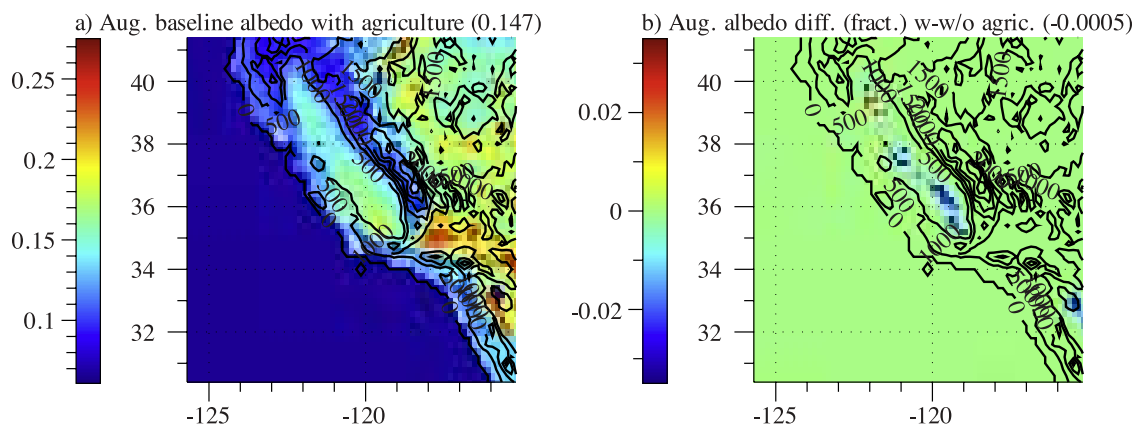


**Figure 2.** August baseline albedo integrated over all 318 solar wavelengths (with agriculture) and the albedo difference in the irrigation-plus-albedo case (w-w/o agric.). The numbers in parentheses are the average albedo or albedo differences (albedo units) over all land points in the figures. Contours are topography.

known (section 2.1). When equation (2) is substituted back into equation (1), equation (1) exactly gives the current “observed” albedo it is constrained by.

[20] Equations (1) and (2) were applied in the absence of agriculture by assuming that the albedo of all land in a soil class in a cell in the absence of agriculture equaled the albedo of land in the same soil class not currently occupied by agriculture. This entailed solving equation (2) with  $f_{ag,i}$ , then setting  $f_{ag,i} = 0$ , then plugging the results from equation (2) for all soil classes into equation (1). The resulting soil-class and grid-cell-averaged albedos were not necessarily the albedo of natural land prior to the introduction of agriculture since much of the nonagricultural land in agricultural areas today has been modified from its natural state. As such,  $A_{non-ag,i}$  can only be defined as the current albedo in the absence of agriculture. Kueppers *et al.* [2007a, 2007b] replaced agricultural land with their nearest-neighbor land use type and assumed a fixed albedo for agriculture. As such, their albedo in the absence of agriculture also represented a current, rather than preagricultural, albedo.

[21] Equation (2) results in plausible value for  $A_{non-ag,i}$  so long as  $A_{ag}$  is known since the equation uses data-constrained values of  $A_{cur}$  and  $f_{ag,i}$ .  $A_{cur}$  is determined from spectral albedo data (section 2.3) and  $f_{ag,i}$ , from high-resolution land use data (section 2.1). The albedo of agricultural crops varies with season and type of crop. Gutman *et al.* [1989] found that the visible albedo of corn in Iowa ranged from 0.12 to 0.14 in spring to 0.2–0.22 in August to 0.18 in September to 0.12 in October. Giambelluca *et al.* [1997] found the albedo of cropland in Brazil to range from 0.17 to 0.176. About 25% of California agriculture is orchards and vineyards [Salas *et al.*, 2006]. The albedo of an apple orchard varies with season from 0.13 to 0.22 [Landsberg *et al.*, 1973]. Here, the albedo of agricultural land was roughly averaged among all crop types to be around  $A_{ag} = 0.20$ , except as discussed next. The agricultural albedo was assumed independent of wavelength due to uncertainty of its wavelength dependence averaged over all crops, and this could be a source of error.

[22] If  $A_{ag}$  is fixed and in error, it can result in  $A_{non-ag,i} < 0$  or  $> 0.4$  in equation (2) when  $A_{cur} - A_{ag}f_{ag,i}$  is small but  $f_{ag,i}$  is large (e.g.,  $> 0.9$ ) or when  $A_{cur} - A_{ag}f_{ag,i}$  is large and  $f_{ag,i} > 0.4$ . To avoid these situations, when  $A_{non-ag,i} < 0.08$  or  $> 0.4$  from equation (2), the equation was resolved using  $A_{ag} = [A_{cur} - A_{na,lim} (1 - f_{ag,i})] / f_{ag,i}$  where  $A_{na,lim} = \min(0.08, A_{cur,i})$  when  $A_{non-ag,i} < 0.08$  and  $\max(0.4, A_{cur})$  when  $A_{non-ag,i} > 0.4$ . This gave a more justifiable estimate of  $A_{non-ag,i}$ . For example, if  $A_{cur} = 0.1$ ,  $A_{ag} = 0.2$ , and  $f_{ag,i} = 0.5$ ,  $A_{non-ag,i} = 0$ , which is unphysical. Applying the correction gives  $A_{ag} = 0.12$  and  $A_{non-ag,i} = 0.08$ , a more realistic solution in that it satisfies equation (2) and ensures that  $A_{ag}$  is still within the range of observed agricultural land albedos.

[23] Figure 2 shows both the baseline albedo (with agriculture) and the albedo difference (with minus without agriculture), derived as described above, weighted by solar flux and summed over all solar wavelengths. The figure shows that agriculture may have increased the solar-integrated albedo of the northern Central Valley by up to 0.035 and decreased that of the southern valley by up to 0.035. Because the maximum grid-cell-averaged changes are no more than  $\pm 0.035$ , the use of equation (1) did not cause significant extreme estimates of albedo. In fact, only 2.2% of nonagricultural albedos at any wavelength or in any soil class from equation (1) were predicted to exceed 0.36.

[24] Although albedo differences here were based on current land use, Figure 2 is somewhat consistent with the fact that, in the 1800s, the northern and middle valleys were mostly marshland (low albedo) and rangeland (moderate albedo) and the southern 15% of the valley below the former Lake Tulare (around  $36^\circ\text{N}$ ) was mostly desert (high albedo) [Kahrl, 1979]. Between the 1800s and the mid 1980s, wetlands in the Central Valley decreased from about 4–5 million acres to about 380,000 acres [Frayer *et al.*, 1989]. For example, Lake Tulare was the largest freshwater lake completely enclosed in the United States, but shrank from about 3100 km<sup>2</sup> in the 1840s to 2000 km<sup>2</sup> in 1868 to about 520 km<sup>2</sup> in 1888, then disappeared [Peet, 1907], due to the diversion of the Kaweah, Kern, Kings, and Tule rivers for agriculture. In sum, the historic conversion to agriculture

is expected to have increased the albedo of the northern valley, caused uncertain effects in the middle valley (more rangeland), and decreased the albedo of the southern valley. The albedo differences in Figure 2, which are albedo differences between current land with and without agriculture, show a similar trend in the northern and southern valley. The middle valley shows a modeled albedo decrease. This may represent the historic change if preagricultural land there was significantly rangeland and had a higher albedo than agriculture.

### 3. Description of Simulations

[25] Nested simulations were run to examine the effects of agriculture in California as a whole (two nested domains) and in the Los Angeles basin (three nested domains). Baseline and sensitivity simulations in both cases were carried out for August 2006.

[26] Anthropogenic gas and particle emissions were derived from the U.S. National Emission Inventory for 2002 [USEPA, 2006a], which accounted for stack, fugitive area, nonroad mobile, and onroad mobile sources. Pollutants emitted hourly included CO, CH<sub>4</sub>, paraffins, olefins, HCHO, CH<sub>3</sub>CHO, higher aldehydes, toluene, xylene, isoprene, NO, NO<sub>2</sub>, HONO, NH<sub>3</sub>, SO<sub>2</sub>, SO<sub>3</sub>, H<sub>2</sub>SO<sub>4</sub>, particle black carbon, particle organic carbon, particle sulfate, and particle nitrate. From the raw U.S. inventory, inventories were prepared for each model domain. Particles were emitted into the model's discrete aerosol size distribution. Additional emission types treated were biogenic gases (isoprene, monoterpenes, other volatile organics from vegetation, and nitric oxide from soils), soil dust, sea spray, pollen, spores, and bacteria, NO from lightning, DMS from the oceans, volcanic SO<sub>2</sub>, many gases and particles from biomass burning, and CO<sub>2</sub>, H<sub>2</sub>, and H<sub>2</sub>O from fossil-fuel combustion and biomass burning.

[27] Emissions from agricultural and other vegetated lands include isoprene, monoterpenes, other organics, pollen, and spores from crops and ammonia/nitrous oxide from fertilizers. Emission rates of these components varied between simulations as a function of meteorological conditions (e.g., isoprene was affected by temperature and radiation; monoterpenes and other organics were affected by temperature; pollen and spores were affected by wind speed and the relative humidity). Emission changes due to vegetation-type changes due to agriculture were not treated.

[28] Sources of black carbon (BC) emissions in the model included shipping, aircraft, other fossil fuels, biofuels, and biomass burning. Land-based fossil-fuel soot (BC, organic matter, and sulfate) emissions were obtained from the USEPA [2006a] within the U.S. and from Bond *et al.* [2004] outside the U.S. Shipping BC emissions were obtained by scaling BC emission factors to the sulfur shipping emission rate from Corbett and Koehler [2003], as described by Jacobson [2006]. Aircraft BC emissions were derived by applying BC emission factors to the 1999 commercial, military, and charter aircraft fuel use data of Sutkus *et al.* [2001] and Mortlock and Van Alstyne [1998]. Soil dust emissions as a function of size, soil type, wind speed, soil moisture, and snow cover were calculated with

the method of Marticorena *et al.* [1997] using soil data from Miller and White [1998].

[29] For both the California and Los Angeles cases, a baseline simulation (with irrigation and current albedo) and two sensitivity simulations, one without irrigation but with current albedo ("no-irrigation") and the other without irrigation and with an estimated albedo without agriculture ("no agriculture"), were run. For the California case, the global domain calculations were the same for both baseline and sensitivity simulations so that errors due to coarser resolution in the global domain did not influence results in the finer California domain. Similarly, for the Los Angeles case, the global and California domain calculations were the same for baseline and sensitivity simulations.

[30] Initial meteorological fields were obtained from Global Forecast System 1° × 1° data for 1 August 2006 [GFS, 2006]. Aerosol and gas fields in all domains were initialized from background data. U.S. EPA ambient air quality data [USEPA, 2006b] for O<sub>3</sub>, CO, NO<sub>2</sub>, SO<sub>2</sub>, PM<sub>2.5</sub>, and PM<sub>10</sub> were then assimilated with background values at the initial time. No data assimilation, nudging, or model spin-up was performed during any simulation. The model has previously been shown to predict immediately the diurnal variation in soil moisture and ambient meteorological and pollutant variables without spin-up or data assimilation [Jacobson, 1999, Figure 2, 1997, 2001b].

[31] Figure 3 here similarly compares baseline model predictions with paired-in-time-and-space data for several gas and aerosol parameters over the August simulation period. The figure demonstrates the predictability of the model over a month. The normalized gross error and normalized bias for ozone >50 ppbv during 39,000 hourly comparisons in California were 28.1% and -0.8%, respectively. California comparisons are provided for meteorological parameters by Jacobson [2001b] and for meteorological/cloud variables by Jacobson *et al.* [2007]. New comparisons with climatological temperature and precipitation are discussed shortly.

### 4. Results for California

[32] Table 2 summarizes statistics for several parameters in California and Los Angeles from the baseline simulation, between the baseline and no-irrigation simulations, and between the baseline and the no-agriculture simulations. Statistics are averages over all grid cells containing any irrigated land in the domain. Such grid cells, contained, on average 8.213% agricultural land, with peaks of 50–90% agricultural land, in the Central Valley. Figure 4 shows some California spatial distributions from the baseline simulation and between the baseline and no-agriculture simulations. The values in parentheses, in this case, are averages over all land (irrigated plus nonirrigated). Table 2 statistics are for different averaging regions than are those in Figure 4 to illustrate that, regional impacts of agriculture are smaller than local impacts. Irrigation data were available for California only, but Figure 1a shows that Nevada has little agricultural land relative to California.

[33] The irrigation of agriculture (without considering albedo differences) increased August soil moisture, averaged over grid cells containing any agriculture in the

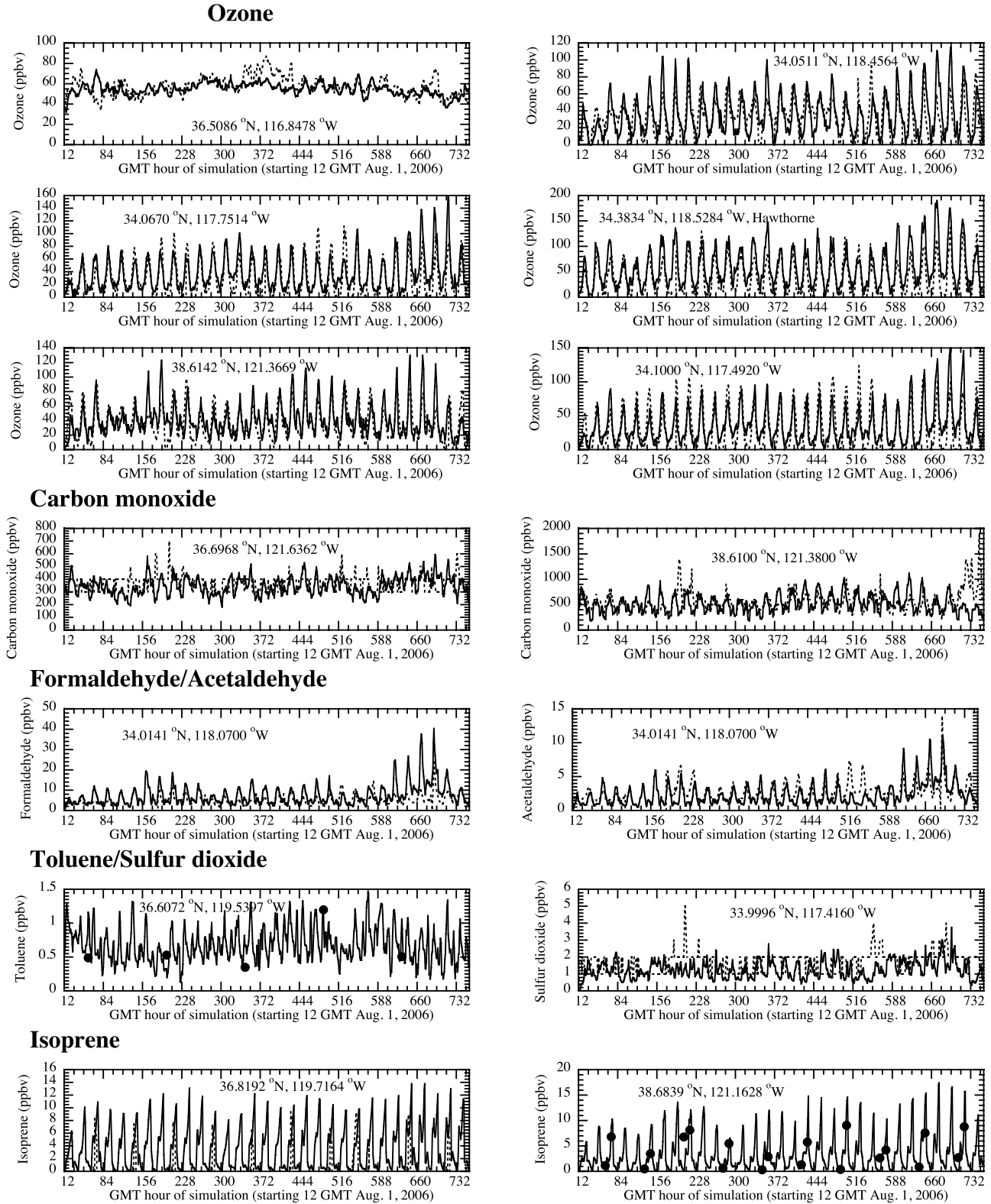


**Figure 3.** Paired-in-time-and-space comparisons of modeled (solid lines) with measured hourly (dashed lines) or sparser (dots) August 2006 ozone, carbon monoxide, formaldehyde, acetaldehyde, toluene, sulfur dioxide, isoprene, particle sulfate, particle black carbon, and sub-10-µm particle mass. Data from USEPA [2006b].

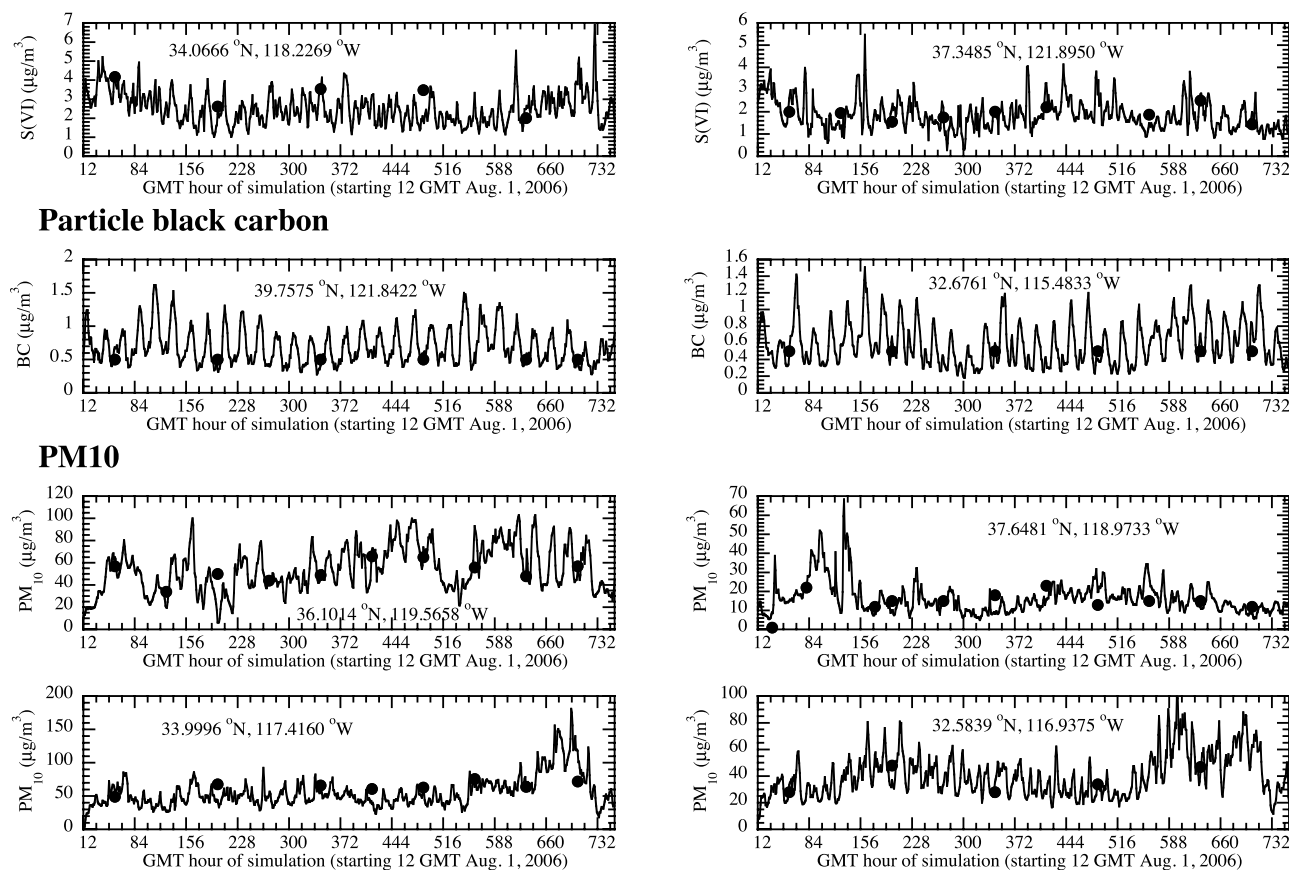


Figure 3. (continued)

California domain, by 20.5% of its preirrigation value of  $0.038 \text{ m}^3/\text{m}^3$  (Table 2). Most of the moisture increases occurred in the Central Valley, where monthly averaged soil moisture increased by up to  $0.11 \text{ m}^3/\text{m}^3$  (Figure 4a). Irrigation of agriculture also occurs in the Imperial Valley (near  $115^\circ\text{W}$ ,  $33^\circ\text{N}$ , Figure 1). However, because this area was predominantly in a five-row buffer area of the California model domain where parameters were relaxed to global-domain values during nesting, feedbacks in the Imperial Valley were dampened and should not be relied on. Soil moisture changes (Figure 4a) occurred over a slightly broader region than irrigation changes (Figure 1) because soil moisture also changed downwind of irrigation due to increases in the relative humidity and moisture deposition downwind.

[34] The increase in soil moisture due to irrigation increased evaporation, which increased water vapor over irrigated land by 2.3%, the relative humidity by 3.9%, and cloud optical depth by 15.2% (Table 2). Increases due to irrigation plus albedo differences were 4.2%, 3.8%, and 5.2% for the same parameters (Table 2). Peak local relative humidity increases in the Central Valley due to irrigation plus albedo differences were 6.5% (Figure 4b). Peak cloud optical depth increases were 0.6 (Figure 4c).

[35] The measured climatological precipitation in the Central Valley and south of the Central Valley (below Bakersfield) in August is low but not zero (Table 3). Modeled precipitation at all 14 locations in the Central

Valley and all 6 locations south of the valley was well within the climatological range (Table 3). Many coarsely resolved regional models overpredict precipitation, as discussed by *Gutowski et al.* [2003]; however, this was not a problem here. August climatological precipitation is generally lower in the middle valley (e.g., mean of 0.03 mm/d in Vacaville and Turlock, 0.04 mm/d in Stockton) than in the northern valley (e.g., 0.13 mm/d, 0.14 mm/d in Chico) or southern valley (e.g., mean of 0.19 mm/d in Barstow). Modeled precipitation was similarly lower in the middle than northern or southern valley. Modeled precipitation was often from nighttime and early morning fog deposits/drizzle and possibly weak, shallow frontal activity, although the fraction of such precipitation was not quantified.

[36] Modeled August baseline 2-m temperatures (same table) were well within August 1971–2000 climatological ranges at 10 out of 20 locations, slightly higher (by no more than 1–1.5 K) than climatological ranges in 7 locations, below climatological values by  $<0.5 \text{ K}$  in 2 locations, and below climatological values by 2 K at one location (Palm Springs) (Table 3). This overall neutral or slightly warm bias differs significantly from results from all four models compared by *Kueppers et al.* [2007a, Figure 2], which exhibited large cool biases of 2–8 K in the Central Valley.

[37] Increases in soil moisture due to irrigation increased the small amount of modeled precipitation by 16.2% over irrigated land between the baseline and no-irrigation simulations (Table 2). With very low precipitation in August, this

**Table 2.** Modeled August-Averaged Baseline Values (With Current Irrigation and Albedo Due to Agriculture) Over All Grid Cells Containing Any Irrigation and Percent Changes in Mean Values Between the Baseline and No-Irrigation Simulations Due (“W-W/O Irrigation”) and Between the Baseline and No Agriculture (No Irrigation and Nonagricultural Albedo) Simulations (“W-W/O Agriculture”)<sup>a</sup>

	California Baseline (W/Agriculture)	California % Change W-W/O Irrigation	California % Change W-W/O Agriculture	SCAB Baseline (W/Agriculture)	SCAB % Change W-W/O Irrigation	SCAB % Change W-W/O Agriculture
Albedo (fraction)	0.127	0	-0.76	0.144	0	-0.20
Soil moisture (m <sup>3</sup> /m <sup>3</sup> )	0.046	+20.53	+20.54	0.028	+15.5	+15.7
Water vapor (kg/kg)	0.007	+2.3	+4.2	0.0064	-0.079	+0.41
Relative humidity (frac.)	0.39	+3.9	+3.8	0.31	-0.61	+0.84
Cloud LWC (g/m <sup>2</sup> )	0.0023	+3.0	+1.5	0.49	-1.6	+1.1
Cloud optical depth	0.39	+15.2	+5.2	0.13	+1.1	-3.4
Cloud fraction	0.041	+19.7	-3.6	0.014	-4.8	-15.5
Precipitation (mm/d)	0.05	+16.2	+5.1	0.007	-2.5	+1.8
Surface solar (W/m <sup>2</sup> )	261	+0.095	+0.098	262	-0.071	-0.094
Surface UV (W/m <sup>2</sup> )	12.3	+1.5	+0.49	12.3	-0.45	-0.63
Surface thermal-IR (W/m <sup>2</sup> )	-118	-1.2	-1.1	-122	-0.12	-0.41
30-m air temperature (K)	296.82	-0.124	-0.017	299.12	+0.042	+0.023
2-m air temp (K) (est.)	297.08	-0.147	-0.055	298.77	-0.006	-0.007
Ground temperature (K)	297.10	-0.148	-0.057	298.74	-0.009	-0.01
Wind speed (m/s)	4.0	+0.61	-0.25	4.03	-0.55	-0.61
BC in precipitation (mg/L)	0.0029	+7.6	+5.4	0.003	+2.5	+2.5
Surface BC (μg/m <sup>3</sup> )	0.82	-1.9	+0.69	2.0	+0.60	+0.63
Column BC (g/m <sup>3</sup> )	0.0007	-4.2	-2.8	0.0013	+1.4	-0.027
Cloud BC (μg/m <sup>3</sup> )	0.007	+9.0	+8.1	0.0077	-2.6	+7.2
Aerosol POM (μg/m <sup>3</sup> )	5.4	-2.1	+0.36	14.1	+0.51	+0.67
Cloud POM (μg/m <sup>3</sup> )	0.043	+10.7	+9.6	0.042	-2.5	+8.1
Aerosol SOM (μg/m <sup>3</sup> )	10.2	-5.7	+0.11	11.3	+0.76	+0.8
Cloud SOM (μg/m <sup>3</sup> )	0.077	+2.5	+4.5	0.011	-6.6	+5.3
Aerosol LWC (μg/m <sup>3</sup> )	3.8	+1.0	+6.3	4.7	-0.08	+4.0
Aerosol S(VI) (μg/m <sup>3</sup> )	0.46	+2.2	+5.2	0.95	+1.9	+2.5
Cloud S(VI) (μg/m <sup>3</sup> )	0.03	+8.5	+9.8	0.030	-3.7	+4.5
Aerosol NH <sub>4</sub> <sup>+</sup> (μg/m <sup>3</sup> )	0.20	+0.55	+8.2	0.28	+0.86	+3.3
Cloud NH <sub>4</sub> <sup>+</sup> (μg/m <sup>3</sup> )	0.009	+5.6	+8.9	0.0073	-4.5	+1.8
Aerosol NO <sub>3</sub> <sup>-</sup> (μg/m <sup>3</sup> )	1.06	-1.0	+4.3	1.8	+3.7	+3.8
Cloud NO <sub>3</sub> <sup>-</sup> (μg/m <sup>3</sup> )	0.036	+6.2	+7.8	0.024	-3.4	+4.5
PM <sub>2.5</sub> (μg/m <sup>3</sup> )	27.6	-3.7	+0.95	39.0	+1.3	+2.0
Column aerosol (g/m <sup>3</sup> )	0.0524	-6.4	-2.8	0.059	+3.0	+4.1
Aerosol optical depth	0.12	-7.2	-4.0	0.14	+1.9	+2.7
Aerosol number (No/cm <sup>3</sup> )	9190	-0.76	-0.6	25,700	+0.34	+0.12
Nitric oxide (ppbv)	0.39	+0.12	+1.5	2.2	+0.064	+1.1
Nitrogen dioxide (ppbv)	2.9	-0.15	+0.29	8.2	+0.16	+0.56
Carbon monoxide (ppbv)	190	-1.3	+0.60	296	+0.41	+0.61
Methane (ppbv)	1710	-0.0025	+0.0012	1725	-0.0012	+0.0006
1,3-butadiene (ppbv)	0.020	-0.27	+0.75	0.069	+0.50	+1.1
Benzene (ppbv)	0.09	+0.56	+2.6	0.19	+0.86	+0.77
PAN (ppbv)	0.92	+0.36	+2.0	0.76	-0.23	-1.1
Nitric acid (ppbv)	0.95	+0.73	+1.67	3.09	+10.1	+10.5
Formaldehyde (ppbv)	5.7	-4.7	+0.81	5.88	+1.5	+0.29
Toluene (ppbv)	0.31	-0.61	+1.3	0.78	+0.79	+0.73
Sulfur dioxide (ppbv)	0.48	-2.6	+0.14	0.97	+0.95	-0.04
Hydroxyl radical (ppbv)	0.000046	+1.4	+0.57	0.000049	-0.31	-0.53
24-h ozone (ppbv)	54.8	-1.7	+0.078	60.1	+0.005	+0.29
Daytime ozone (ppbv)	64.0	-1.5	+0.063	75.1	-0.26	+0.052

<sup>a</sup>Results correspond to several of the panels in Figures 4 and 6. Grid cells containing any agriculture comprised 23.75% and 41.97% of the entire areas of the California and SCAB domains, respectively, and the fraction of irrigated agricultural land in such cells was about 8.213% and 1.829%, respectively.

increase was not much water. In the baseline minus no-agriculture simulations, precipitation increased by 5.2% over irrigated land with most changes occurring in the Central Valley (Table 2 and Figure 4d).

[38] The increase in drizzle and cloud water in the Central Valley due to agriculture increased the concentration of pollutants in precipitation and clouds, increasing wet removal of these pollutants. For example, irrigation plus

**Figure 4.** (a–d) Modeled August-averaged (left) baseline values (with irrigation and current albedo of agriculture) and (right) baseline values minus those without irrigation and with an estimated albedo before agriculture (w-w/o agric.) for several parameters in the California domain. The number in parentheses is the average over all land points in the figure. Land comprises 51.06% of the area in each diagram. Contours are topography. (e–j) Same as Figures 4a–4d but for additional parameters.

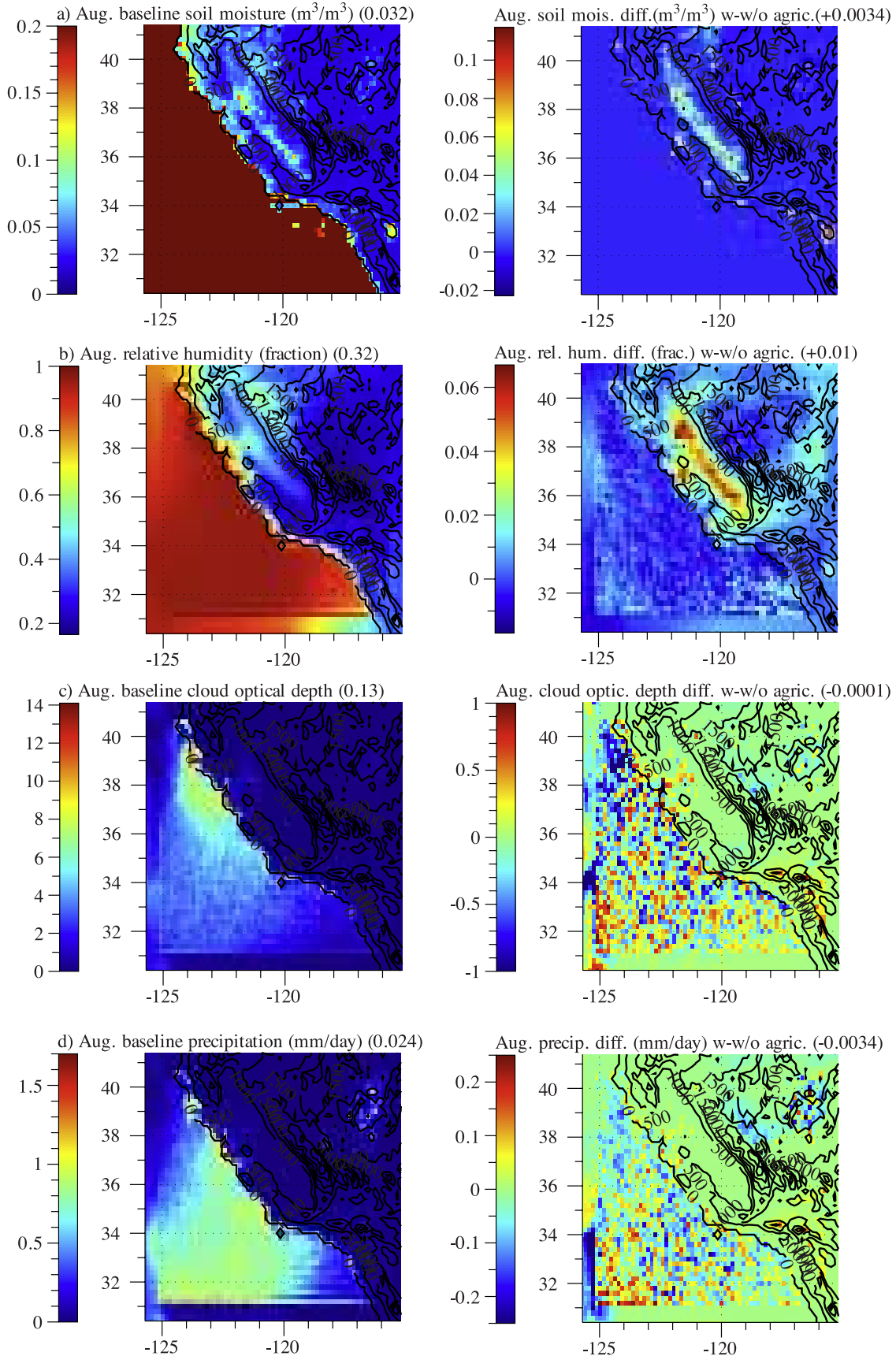


Figure 4

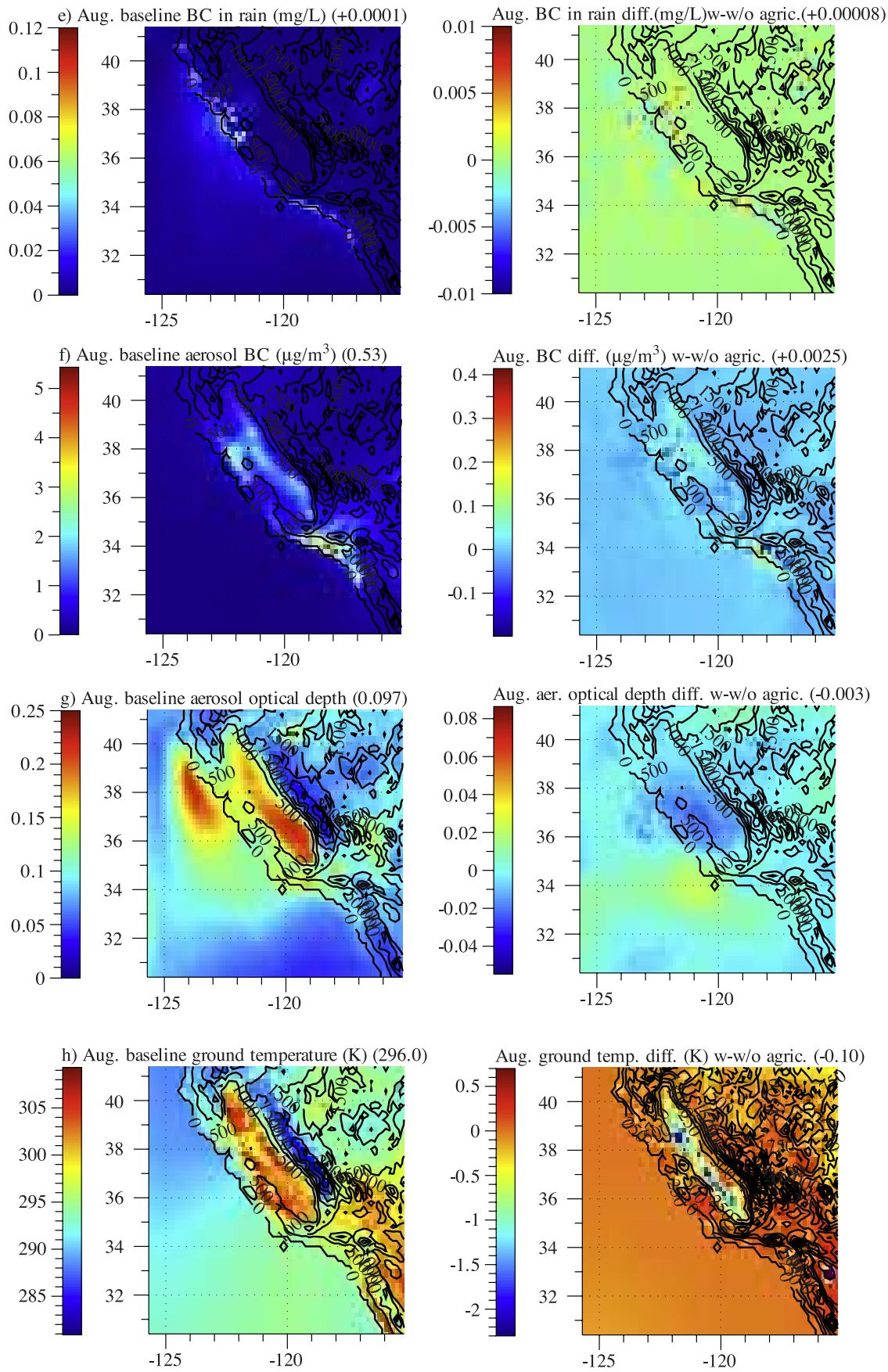


Figure 4. (continued)

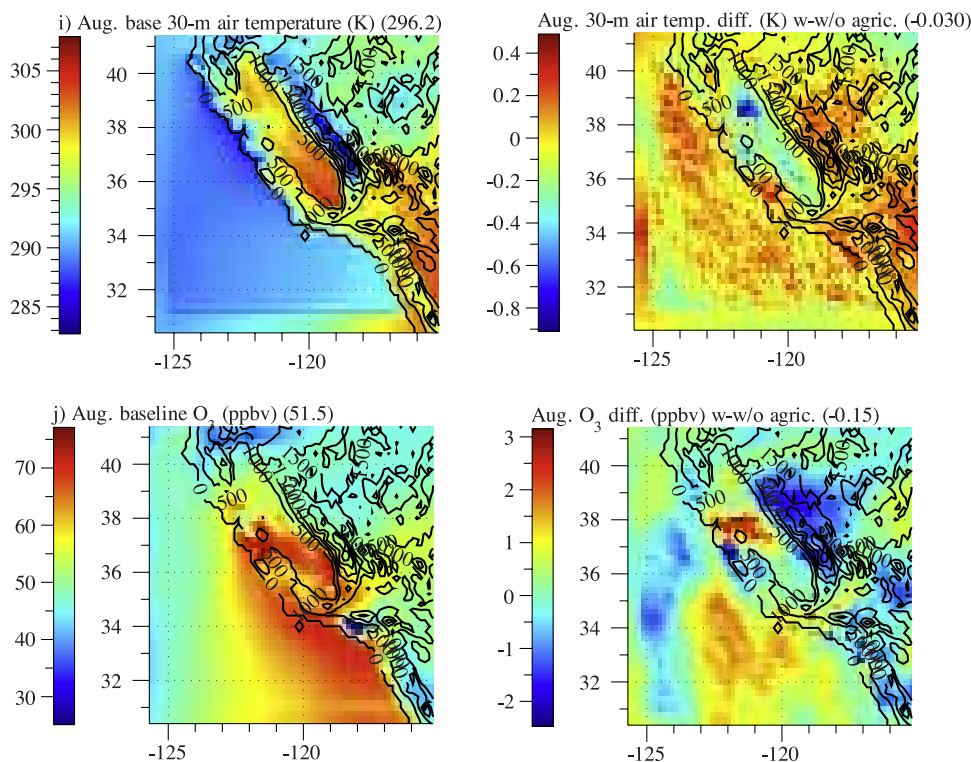


Figure 4. (continued)

albedo differences increased the concentration of BC in cloud water by 8.1% (Table 2) and rainwater by 5.4% (Table 2 and Figure 4e), decreasing column aerosol BC by 2.8% (Table 2). Because irrigation plus albedo differences stabilized near-surface air by cooling the ground more than the air (Table 2), near-surface BC and other aerosol components increased (Figure 4f and Table 2).

[39] Owing to enhanced drizzle and clouds, irrigation plus albedo differences similarly decreased column aerosol mass by 2.8% (Table 2), aerosol extinction (Table 2), aerosol optical depth (Table 2 and Figure 4g), and aerosol number (Table 2). Offshore aerosol optical depth at about 34°N increased by about 0.03 (Figure 4g) due to the increase sea spray emissions caused by a slight 0.1–0.2 m/s

**Table 3.** August (Day and Night) Climatological (1971–2000) and Modeled Precipitation and 2-m Air Temperature at Several Stations (From North to South) in the Central Valley and South of the Valley (Barstow and Below)<sup>a</sup>

Station	Latitude (deg)	Longitude (deg)	Climatological Precipitation (mm/d)	Modeled Precipitation (mm/d)	Climatological 2-m Temperature (K)	Modeled Temperature (K)
Orland	39.75	122.20	0.13 (0–1.07)	0.0002	298.15 (295.6–300.0)	299.8
Chico	39.70	121.82	0.14 (0–1.25)	0	297.3 (294.5–299.1)	300.1
Willows	39.52	122.18	0.08 (0–0.68)	0.0023	297.1 (295.3–299.0)	300.5
Oroville	39.50	121.57	0.14 (0–1.27)	0	297.7 (295.7–300.0)	300.6
Colusa	39.22	122.00	0.04 (0–0.5)	0.009	297.3 (295.9–298.6)	300.3
Sacramento	38.58	121.50	0.04 (0–0.48)	0.023	297.9 (296.15–300.2)	298.2
Vacaville	38.37	122.00	0.03 (0–0.55)	0.016	297.8 (296.2–299.5)	297.5
Stockton	37.95	121.23	0.04 (0–0.55)	0.019	296.7 (294.8–298.9)	297.4
Turlock	37.48	120.85	0.03 (0–0.47)	0	297.9 (295.7–300.3)	299.5
Madera	36.97	120.02	0.02 (0–0.11)	0	299.0 (296.0–300.5)	301.4
Visalia	36.33	119.30	0.017 (0–0.11)	0	298.7 (296.2–300.2)	302.5
Kern River	35.47	118.78	0.08 (0–0.8)	0	303.4 (299.3–305.2)	301.2
Bakersfield	35.42	119.05	0.07 (0–1.0)	0	300.9 (298.5–302.6)	303.7
Barstow	34.90	117.02	0.19 (0–1.29)	0.02	302.2 (299.5–304.3)	298.8
Daggett	34.87	116.78	0.33 (0–2.19)	0.01	303.4 (300.6–305.8)	300.2
Fontana	34.08	117.50	0.09 (0–1.62)	0.012	299.3 (296.6–302.9)	298.7
LA Apt.	33.93	118.40	0.12 (0–2.09)	0.10	294.7 (293.0–296.9)	294.2
Anaheim	33.90	117.87	0.01 (0–0.14)	0.014	296.7 (294.3–298.8)	298.1
Palm Springs	33.90	116.55	0.34 (0–3.66)	0.006	306.2 (303.1–308.8)	301.5
Sun City	33.72	117.20	0.21 (0–1.72)	0.011	299.2 (296.8–301.9)	299.5

<sup>a</sup>Climatological data were from the *Western Regional Climate Center* [2006].

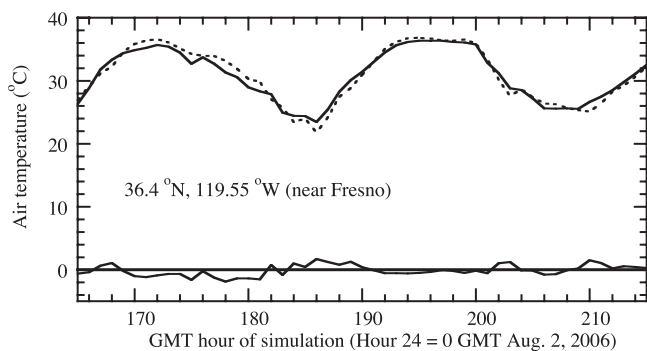


**Figure 5.** Time-dependent variation during 2 days in August of modeled near-surface air temperature near Fresno, California, when irrigation was included (solid line) and excluded (dashed line). The solid curve near the bottom is the difference.

increase in offshore wind speed, caused by a change in pressure gradients triggered by changes in temperature profiles over land versus water due to changes in irrigation.

[40] The decrease in aerosol extinction due to irrigation plus albedo differences slightly increased surface solar and UV irradiances to a greater extent than increases in cloud fraction decreased such irradiances in the Central Valley (Table 2). This occurred because cloud fractions were so low so changes in them had little impact. The increase in water vapor and decrease in ground temperature increased the net downward (decreased net upward) thermal-IR there (Table 2).

[41] Despite the subtle radiation increase in the Central Valley, the increase in soil moisture due to irrigation decreased 2-m air temperatures by an irrigated-land average of 0.43 K (0.15%, Table 2). The net albedo decrease (Table 2) combined with increased irrigation due to agriculture reduced the 2-m cooling from agriculture to 0.16 K (0.055%, Table 2), averaged over irrigated-land. Thus, albedo differences had a measurable impact on offsetting the temperature decrease due to irrigation.

[42] The temperature decrease over all land in the model domain due to irrigation-plus albedo differences at the ground was 0.1 K (Figure 4h) and at 30 m was 0.03 K (Figure 4i). These were both 40% lower than the ground cooling of 0.17 K (0.057%) and 30-m cooling of 0.05 K (0.017%) (Table 2), respectively, over all model cells containing any agriculture and much lower than the peak temperature decreases due to irrigation-plus- albedo differences of 2.3 K at the ground (Figure 4h) and 0.9 K at 30 m (Figure 4i). This suggests that agriculture had greater local than regional temperature effects during the short simulations.

[43] Irrigation cooled the air on average over day and night by cooling more during the day than warming during the night. One example of this is given for illustration in Figure 5. In general, irrigation reduced temperature maxima and increased temperature minima.

[44] The net cooling and precipitation increase due to irrigation plus albedo differences found here are consistent in direction with the data analysis results of *Barnston and Schickedanz* [1984] and *Moore and Rojstaczer* [2001]. The cooling is also consistent in direction with results from

*Adegoke et al.* [2003, 2007], *Boucher et al.* [2004], *Kueppers et al.* [2007a, 2007b], *Lobell et al.* [2006], and *Bonfils and Lobell* [2007].

[45] *Kueppers et al.* [2007b] (hereinafter referred to as K07) used several regional climate models to estimate a net decrease in the August day-night mean 2-m temperature of  $-1.4$  to  $-3.1$  K and an increase in the relative humidity of 9 to 36% due to irrigation alone over all irrigated agricultural land in the western U.S.. Here, the August 2-m temperature and relative humidity changes over grid cells containing irrigation ( $-0.43$  K and  $+3.9\%$ ) were in the same direction but smaller in magnitude, for several explainable reasons.

[46] First, the models compared by K07 all used much higher irrigation rates than the data-derived rates used here. The model with the lowest irrigation rate in K07 assumed a constant rate of  $4.8225 \times 10^{-8}$   $\text{m}^3/\text{m}^2/\text{s}$  over irrigated land, about 2.64 times higher than that used here from *Salas et al.* [2006] over irrigated land in August (section 2.2). This resulted in a total August irrigation rate in K07 of 7.44 billion  $\text{m}^3/\text{August}$  compared with 2.18 billion  $\text{m}^3/\text{August}$  here (where the total domain size was slightly smaller). The other models in K07 implicitly assumed higher irrigation rates than the first by specifying soil moisture always at saturation or field capacity, respectively, over irrigated land.

[47] Second, the models of K07 were up to 3 times coarser resolution than that used here (e.g., 900  $\text{km}^2/\text{grid cell}$  for the K07 model with the lowest irrigation rate versus 300  $\text{km}^2/\text{grid cell}$  here), and irrigation was applied evenly over each entire grid cell containing any agriculture in K07, whereas irrigation here was applied proportionally to the fraction of agricultural land in each subgrid soil class of each grid cell. As such, irrigation was applied to a smaller percent of each grid cell containing agriculture here. Thus, the results provided in Table 2 here, which are averages over grid cells containing anywhere from 0.001% to 90% irrigated land, were lower in magnitude than were results in K07, which were averages over grid cells containing an assumed 100% irrigated land.

[48] Additionally, the irrigation rates here varied daily, decreasing by almost a factor of three between the beginning and end of August (section 2.2). The rates in K07 were applied uniformly over the month. A more intense period of irrigation followed by low irrigation results in less cooling than constant irrigation over a month since, once the soil is saturated (as with intense irrigation), the cooling rate slows since specific heat of a soil-water mixture cannot rise further (and runoff drains excess moisture). This intense period of cooling must be averaged with a period of low moisture. A constant irrigation rate, on the other hand, results in a longer period of intense cooling and less runoff. Further, the soil model used here contained 10 layers, treating layer-by-layer moisture and energy diffusion and water drainage between layers for each subgrid soil type. The models in K07 used 2, 3, or 4 soil layers, and none treated moisture or energy diffusion separately for each subgrid soil type in each grid cell.

[49] The factors above resulted in soil moisture increases over all California land containing any agriculture in K07's lowest case of  $0.18$   $\text{m}^3/\text{m}^3$  in August. This compares with an average increase of about  $0.009$   $\text{m}^3/\text{m}^3$  here (Table 2).

Most of this factor of 20 difference can be accounted for by considering that K07 used an irrigation rate 2.64 times higher and spread their irrigation over a total area 5 times more concentrated than here since irrigation here was spread at the subgrid scale over more and smaller cells, decreasing the buildup of moisture when averaging over nonirrigated and irrigated parts of cells. In K07, 100% of large cells were irrigated, so the average moisture in such cells was large. The maximum soil moisture changes in the present study were  $0.11 \text{ m}^3/\text{m}^3$  in parts of the Central Valley, confirming that, in areas where irrigation is concentrated, effects such as found in K07 are possible. This is further confirmed by the fact that the spatial maximum day-night average cooling here (0.9 K at 30 m and 2.3 K at the ground) is close to that of K07 (1.4 to 3.1 K).

[50] The models of K07 resulted in cool biases of 2–8 K in the Central Valley whereas the present model did not (Table 3). K07 state that the cool biases “suggest that soil moisture is prescribed to be too high where irrigation is specified or the resolution of the models... is too coarse to capture the spatial variation in land use.” This conclusion is consistent with the analysis above.

[51] K07 (Table 3) found that land use change due to agriculture caused a 2-m temperature change of  $-0.3$  to  $+1.1$  K among the models compared. Here, the change in albedo due to agriculture caused a net 2-m air temperature increase over irrigated land of about  $+0.27$  K, reducing the average 2-m cooling over irrigated land from 0.43 K to 0.16 K (Table 2). The direction of the albedo effect is similar to that found in K07.

[52] *Bonfils and Lobell* [2007] (hereinafter referred to as BL07) analyzed historic temperature data to estimate the local impact of irrigation in the Central Valley. They considered two data sets at high resolution ( $0.125^\circ$ ) and two at low resolution ( $0.5^\circ$ ). Results indicate a day-night average temperature change that BL07 attribute to historic agriculture, of 0.74 to 2.4 K (0.057 to 0.186 K/decade) in regions on average, 75% irrigated. The present paper found, by cause and effect simulations, a spatial maximum day-night-average cooling due to agriculture (irrigation plus albedo differences) in highly irrigated regions of the Central Valley of 2.3 K at the ground (Figure 4h) and 0.9 K at 30 m (Figure 4i), both within the range of BL07.

[53] Because the warming due to albedo differences from agriculture found here offset only part of the cooling due to irrigation in the Central Valley, the net warming found in the valley by *Christy et al.* [2005] is probably not due to agriculture, as speculated therein, but to anthropogenic greenhouse gases and particulate black carbon.

[54] Finally, ozone decreased over irrigated land with irrigation alone but increased with irrigation plus albedo differences (Figure 4j and Table 2). In the former case, ozone decreased in the Central Valley due to reductions there in several precursors, such as formaldehyde and toluene (Table 2), because of more clouds and precipitation in that case (Table 2). In the latter case, ozone increased primarily in the mid-Central Valley (Figure 4j), because PAN increased there due to a temperature decrease, since PAN thermally decomposes less at lower temperature. The PAN increase removed  $\text{NO}_x$ , increasing ozone, since  $\text{NO}_x$  titrates ozone. PAN did not increase much due to irrigation

alone because of greater clouds and precipitation due to irrigation in that case.

[55] Decreases in column aerosol due to irrigation and irrigation plus albedo differences increased surface UV radiation and water vapor over irrigated land (Table 2). Increases in UV and water vapor increased OH (Table 2), increasing the oxidation rate of several chemicals. Higher water vapor also increased ozone at high ozone but decreased or caused little change at low ozone, as explained chemically by *Jacobson* [2008]. Conversely, lower temperatures decreased ozone at high ozone but had little effect at low ozone due to the temperature dependence of reactions (*ibid.*).

[56] Finally, irrigation and irrigation plus albedo differences slightly increased near-surface concentrations of several aerosol components, particularly in the middle and northern Central Valley, while reducing the column loadings of these components. For example, whereas column aerosol decreased by 2.8% in the irrigation plus albedo case, near-surface  $\text{PM}_{2.5}$  increased by about 1% (Table 2). The near-surface aerosol increase can be seen with respect to BC in Figure 4f. Cooler ground temperatures due to irrigation stabilized the air, reducing mixing depths and near-surface wind speeds over irrigated land, particularly in the middle and northern valley (figure not shown), increasing near-surface concentrations. The reduction in near-surface wind speed with increasing soil moisture is consistent with results from *Jacobson* [1999]. However, here irrigation increased cloud water and precipitation, increasing the scavenging and cloud water concentrations of aerosol particles and soluble gases, decreasing the ambient levels of these particles and gases aloft or offsetting their increases near the surface (Table 2). Table 2 indicates that irrigation enhanced clouds and precipitation thus reduced pollution more (or increased it less) than irrigation plus albedo differences, most likely due to slightly cooler air due to irrigation alone. In sum, agriculture decreased column pollution when clouds and precipitation were present by increasing such clouds and precipitation and offsetting some or all surface pollution increases from reduced stability and dispersion.

## 5. Results for the SCAB (Los Angeles)

[57] Agriculture and irrigation in the Los Angeles basin occur primarily in the eastern basin but are distributed sparsely (Figures 1b and 1d). Agriculture was calculated to decrease albedo on average, primarily in the southernmost Central Valley (north of the basin), the eastern basin, and east of the San Bernardino Mountains (figure not shown). Very small albedo increases occurred in some locations of agriculture in Figure 1b.

[58] As in California, irrigation plus albedo differences in Los Angeles increased soil moisture (Figure 6a), water vapor (Table 2), and the relative humidity (Figure 6b). The baseline cloud optical depth (Figure 6c) and precipitation (primarily drizzle from fog) (Figure 6e) were small over land (1/10 and 1/3 of those in California as a whole), so changes in these parameters were also small and dominated by changes near the coast (Figures 6d and 6f). Changes in solar, UV, and thermal-IR due to agriculture were also small (Table 2).

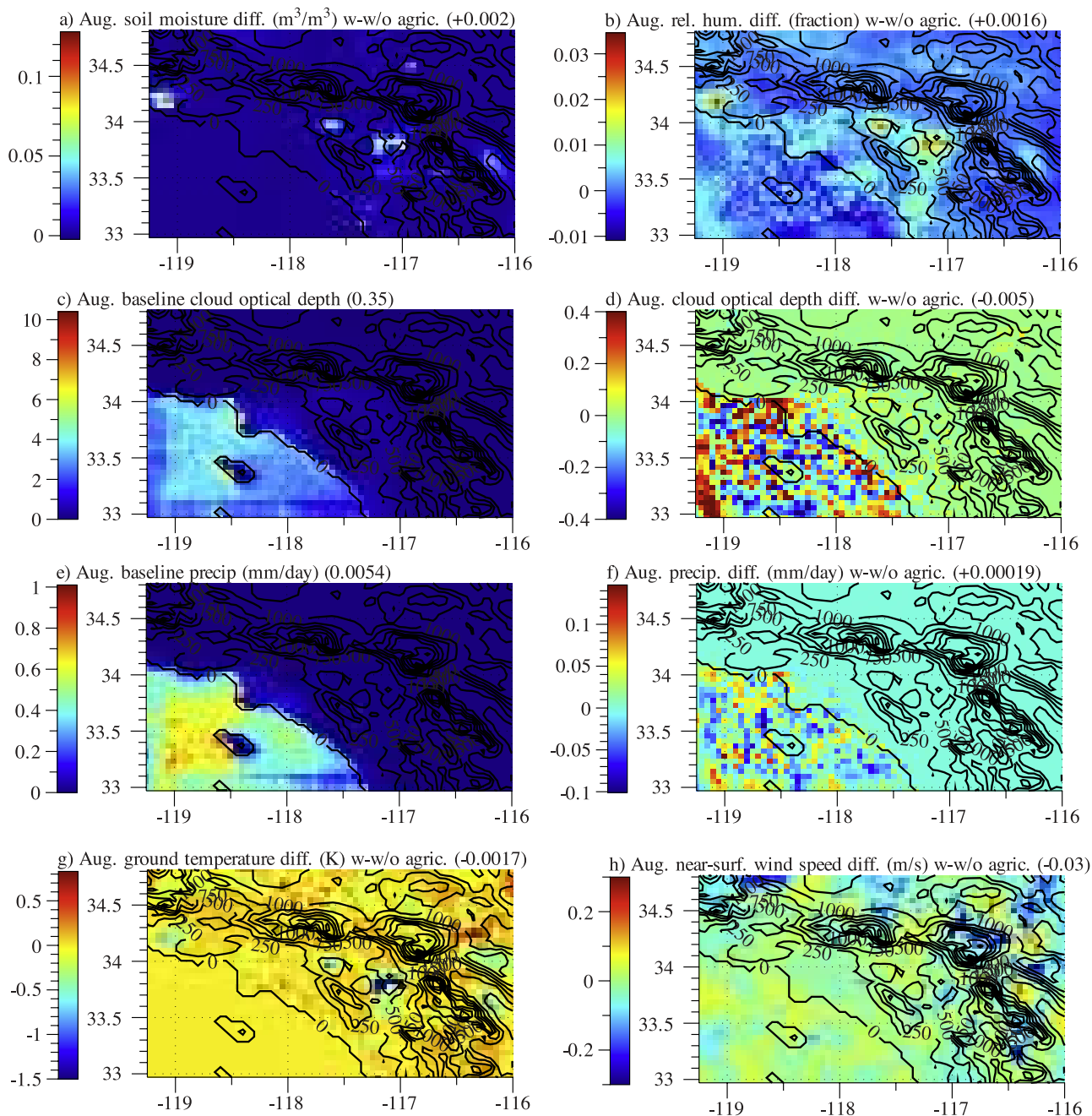


**Figure 6.** (a–h) Modeled August-averaged differences in several parameters between the baseline case and the case without irrigation and with an estimated albedo before agriculture (w/w/o agric.) in the SCAB (Los Angeles) model domain. The baseline cloud optical depth and precipitation are also shown. The number in parentheses is the average over all land points in the figure. Land comprises 75% of the area in each diagram. Contours are topography. (i–l) Same as Figures 6a–6h, but for additional parameters.

[59] As in California, agriculture in Los Angeles decreased ground temperatures, most notably near irrigated land (Figure 6g and Table 2). The average decrease, though, was 5–15 times smaller than that in the Central Valley (Table 2). The decrease in ground temperature stabilized the air, reducing turbulent kinetic energy and shearing stress, slowing the winds (Figure 6h and Table 2), reducing the advection of cool ocean air to the land, slightly increasing 30-m air temperatures (Table 2) and stabilizing the air further in a positive feedback loop.

[60] Stabilization of the air and lower wind speed reduced dispersion, increasing the near-surface concentrations of all particle and most gas pollutants (Table 2), including BC (Figure 6i), primary and secondary organic matter (POM and SOM), sulfate, nitrate, ammonium (Table 2),  $\text{PM}_{2.5}$  (Figure 6j), aerosol number, CO,  $\text{CH}_4$ , NO,  $\text{NO}_2$  (Figure 6k),  $\text{HNO}_3$ ,  $\text{C}_4\text{H}_6$ ,  $\text{C}_6\text{H}_6$ , toluene, and  $\text{O}_3$  (Figure 6l) among others.  $\text{SO}_2$  decreased due primarily to a slight increase in precipitation near the coast, where most  $\text{SO}_2$  is emitted in Los Angeles. Although ozone increased on average in Los

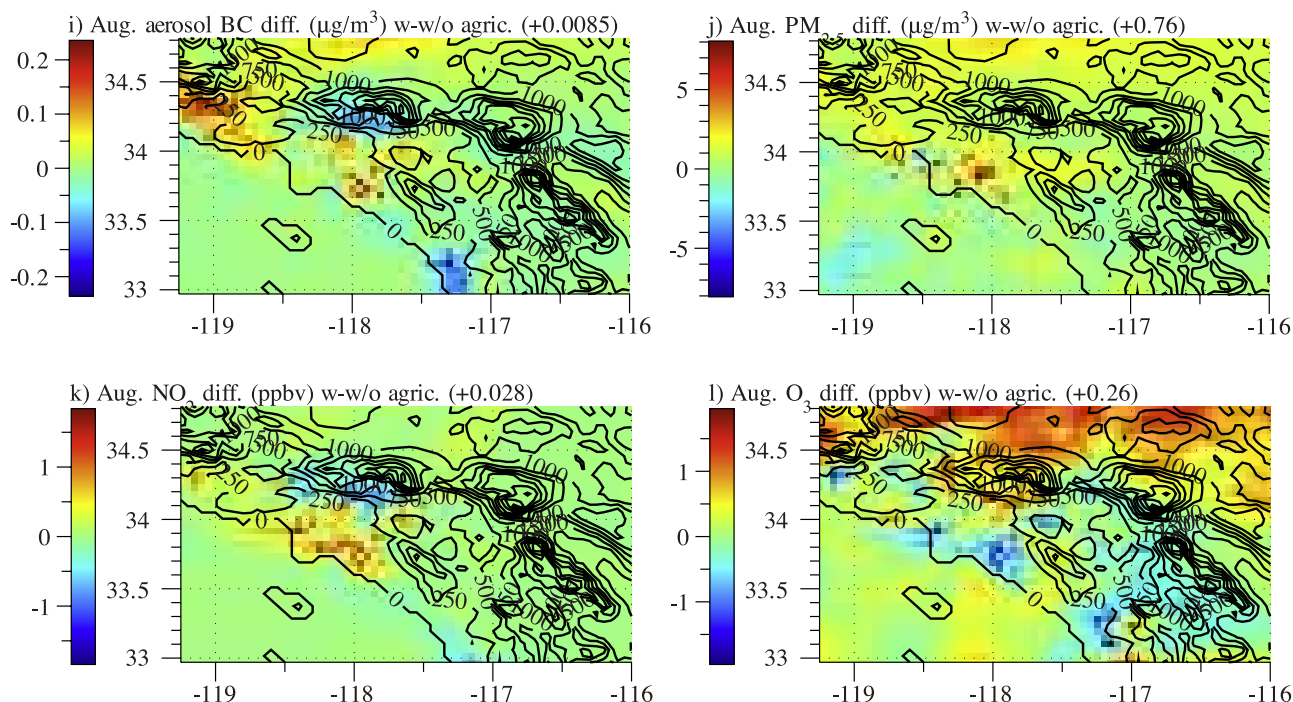


Figure 6. (continued)

Angeles and particularly in the eastern basin, ozone decreases occurred (Figure 6l) in locations where  $\text{NO}_x$  increased the most due to agriculture (e.g., Figure 6k). These were mostly locations of heavy  $\text{NO}_x$  emissions, because the enhanced  $\text{NO}_x$  titrated ozone. The slightly higher air temperature due to agriculture caused some additional PAN to thermally decompose compared with the baseline case (Table 2).

[61] The increase in cloud water due to irrigation plus albedo differences (Table 2) increased aerosols within clouds (Table 2). This occurred more in California as a whole due to the greater cloudiness in California as a whole than in Los Angeles (Table 2).

[62] Previously, *Jacobson* [1999] studied the effect of soil moisture changes on air pollution in Los Angeles without considering feedbacks to clouds and precipitation. That study found that an increase in soil moisture in Los Angeles cooled the ground, stabilizing the air, increasing the concentrations of many primary pollutants by reducing vertical mixing and slowing winds. Here, the changes in soil moisture in Los Angeles were much smaller and more spatially variable than in the work of *Jacobson* [1999], where initial soil moisture was specified and uniform spatially. Nevertheless, the effects found here due to irrigation (and irrigation plus albedo differences) were similar. Namely, in the absence of significant cloudiness, agriculture reduced ground temperatures, stabilizing the air, slowing wind speeds, and increasing the concentrations of particles and gases.

## 6. Additional Analysis

[63] Two additional pairs of California simulations were run, with and without agriculture (irrigation plus albedo differences), with a different start date (30 and 31 July 2006) and initial GFS data for each start date. Mean soil

moisture, relative humidity, and 30-m air temperatures changes over irrigated grid cells in the two cases were as follows: 30 July: +17.8%, +3.3%, and  $-0.009\%$ , respectively; 31 July: +17.3%, +3.9%, and  $-0.024\%$ . These compare with +20.5%, +3.8%, and  $-0.017\%$ , respectively for the 1 August case (Table 2). This consistency in order of magnitude and direction of results across an ensemble of start dates provides support that the results are not random or noise but real model responses to irrigation and/or albedo differences. The magnitudes of the changes are more uncertain and may change upon an improvement in model resolution and physical processes treated. For example, the use of a nonhydrostatic versus hydrostatic model with 1 km rather than 5- or 15-km resolution would improve treatment of convective cloud processes; a better quantification of preagricultural land use would also improve estimates of albedo differences; a simulation period longer than a month or for different Augusts would improve statistical significance of the results; a more highly resolved representation of irrigation (hourly instead of daily) would improve estimates of soil moisture variations and temperature response.

## 7. Conclusions

[64] This paper discussed effects of irrigation and albedo differences due to agriculture on California and Los Angeles air pollution and climate over one August. High-resolution albedo and irrigation data were combined at the subgrid scale in numerical simulations to examine the impacts. An inversion method was applied to the albedo data to estimate California's albedo in the absence of agriculture. If this estimate is correct, agriculture may increase the albedo of the northern Central Valley but decrease that of the southern valley relative to land use today in the absence of agriculture.

[65] From the simulations, irrigation and albedo differences due to agriculture were found to impact air quality and short-term climate. Irrigation alone decreased day-plus-night 2-m air temperatures by about 0.43 K over irrigated land in California. Irrigation plus albedo differences decreased temperatures by less, 0.16 K because warming from the net decrease in albedo partially offset cooling due to the irrigation increase. Irrigation alone increased nighttime temperatures but decreased daytime temperatures to a greater extent. The spatial maximum day-night average August cooling due to irrigation plus albedo differences from agriculture was 0.9 K at 30 m and 2.3 K at the ground, occurring in the Central Valley. This is in the range of an historic 0.74–2.4 K cooling at 2 m attributed to heavily irrigated agriculture in an independent data analysis study. Because the warming due to albedo differences from agriculture found here offset only part of the cooling due to irrigation in the Central Valley and because aerosol particles cause a net cooling in the valley, the net historic warming of the overall valley is probably due to anthropogenic greenhouse gases and black carbon rather than an increase in agriculture. Irrigation in California increased the otherwise low soil moisture over irrigated land by about 20%, the relative humidity by 4%, cloud optical depth by 5%, and drizzle by 5% (Table 2).

[66] By slightly enhancing clouds and drizzle in the Central Valley, agriculture shifted the aerosol and soluble gas mass to clouds and precipitation there. In Los Angeles and the Central Valley, irrigation stabilized surface air. In the absence of clouds, this slowed surface winds and reduced vertical turbulence, increasing aerosol and gas concentrations. Thus, in the absence of significant clouds and precipitation, agriculture can increase pollution by reducing pollution dispersion. Conversely, when clouds and precipitation are present, increases in both due to agriculture can reduce or offset pollution increases. Some chemically or thermally active pollutants, such as ozone, are sensitive to how agriculture changes their precursors. In emission source regions of Los Angeles, for example, an increase in near-surface  $\text{NO}_x$  due to reduced dispersion caused by agriculture enhanced ozone titration. In  $\text{NO}_x$ -poor areas, such as in parts of the polluted eastern Los Angeles basin, though, reduced dispersion from agriculture increased ozone and particulate matter. Overall, agriculture increased  $\text{PM}_{2.5}$  by ~2% and ozone by ~0.1% near or over irrigated agriculture in Los Angeles. The  $\text{PM}_{2.5}$  increases, in particular, are of concern since  $\text{PM}_{2.5}$  is the most unhealthy component of air pollution.

[67] **Acknowledgments.** This work was funded by California Energy Commission's Public Interest Energy Research Environmental Area (PIREA) program and by NASA under grants NNG04GE93G and NNG04GJ89G. I would like to thank Guido Franco for helpful comments, William Salas for providing irrigation data, and John Ten Hoeve for generating several surface data files.

## References

- Adegoke, J. O., R. A. S. Pielke, J. L. Eastman, R. Mahmood, and K. G. Hubbard (2003), Impact of irrigation on midsummer surface fluxes and temperature under dry synoptic conditions: A regional atmospheric model study of the U.S. High Plains, *Mon. Weather Rev.*, *131*, 556–564, doi:10.1175/1520-0493(2003)131<0556:IOIOMS>2.0.CO;2.
- Adegoke, J. O., R. Pielke Sr., and A. M. Carleton (2007), Observational and modeling studies of the impacts of agriculture-related land use change on planetary boundary layer processes in the central U.S., *Agric. For. Meteorol.*, *142*, 203–215, doi:10.1016/j.agrformet.2006.07.013.
- Barnston, A., and P. T. Schickedanz (1984), The effect of irrigation on warm season precipitation in the southern Great Plains, *J. Clim. Appl. Meteorol.*, *23*, 865–888, doi:10.1175/1520-0450(1984)023<0865:TEOIEW>2.0.CO;2.
- Bond, T. C., D. G. Streets, K. F. Yarber, S. M. Nelson, J.-H. Woo, and Z. Klimont (2004), A technology-based global inventory of black and organic carbon emissions from combustion, *J. Geophys. Res.*, *109*, D14203, doi:10.1029/2003JD003697.
- Bonfils, C., and D. Lobell (2007), Empirical evidence for a recent slowdown in irrigation-induced cooling, *Proc. Natl. Acad. Sci. U. S. A.*, *104*, 13,582–13,587, doi:10.1073/pnas.0700144104.
- Boucher, O., G. Myhre, and A. Myhre (2004), Direct human influence of irrigation on atmospheric water vapor and climate, *Clim. Dyn.*, *22*, 597–603, doi:10.1007/s00382-004-0402-4.
- Christy, J. R., W. B. Norris, K. Redmond, and K. P. Gallo (2005), Methodology and results of calculating Central California surface temperature trends: Evidence of human-induced climate change?, *J. Clim.*, *19*, 548–563, doi:10.1175/JCLI3627.1.
- Corbett, J. J., and H. W. Koehler (2003), Updated emissions from ocean shipping, *J. Geophys. Res.*, *108*(D20), 4650, doi:10.1029/2003JD003751.
- Cuenca, R. H., M. Ek, and L. Mahrt (1996), Impact of soil water property parameterization on atmospheric boundary layer simulation, *J. Geophys. Res.*, *101*, 7269–7277, doi:10.1029/95JD02413.
- Emori, S. (1998), The interaction of cumulus convection with soil moisture distribution: An idealized simulation, *J. Geophys. Res.*, *103*, 8873–8884, doi:10.1029/98JD00426.
- Fan, Y., and H. van den Dool (2004), Climate Prediction Center global monthly soil moisture data set at 0.5° resolution for 1948 to present, *J. Geophys. Res.*, *109*, D10102, doi:10.1029/2003JD004345.
- Fennessy, M. J., and J. Shukla (1999), Impact of initial soil wetness on seasonal atmospheric prediction, *J. Clim.*, *12*, 3167–3180, doi:10.1175/1520-0442(1999)012<3167:IOISWO>2.0.CO;2.
- Frayer, W. E., D. D. Peters, and H. R. Pywell (1989), Wetlands of the California Central Valley: Status and trends-1939 to the mid-1980s, 28 pp., U.S. Fish and Wildlife Serv., Region 1, Portland, Ore.
- Giambelluca, T. W., D. Holscher, T. X. Bastos, R. R. Frazao, M. A. Nullet, and A. D. Ziegler (1997), Observations of albedo and radiation balance over postforest land surfaces in the Eastern Amazon basin, *J. Clim.*, *10*, 919–928, doi:10.1175/1520-0442(1997)010<0919:OOAARB>2.0.CO;2.
- Global Forecast System (GFS) (2006), National Center for Environmental Prediction, <http://nomads.nccdc.noaa.gov/data/gfs-avn-hi/>.
- Gutman, G., G. Ohring, D. Tarpley, and R. Ambroziak (1989), Albedo of the U.S. Great Plains as determined from NOAA-9 AVHRR data, *J. Clim.*, *2*, 608–617, doi:10.1175/1520-0442(1989)002<0608:AOTUGP>2.0.CO;2.
- Gutowski, W. J., Jr., S. G. Decker, R. A. Donavon, Z. Pan, R. W. Arritt, and E. S. Takle (2003), Temporal-spatial scales of observed and simulated precipitation in central U.S. climate, *J. Clim.*, *16*, 3841–3847, doi:10.1175/1520-0442(2003)016<3841:TSSOAS>2.0.CO;2.
- Jacobson, M. Z. (1997), Development and application of a new air pollution modeling system. Part III: Aerosol-phase simulations, *Atmos. Environ.*, *31B*, 587–608, doi:10.1016/S1352-2310(96)00201-4.
- Jacobson, M. Z. (1999), Studying the effects of soil moisture on ozone, temperatures, and winds in Los Angeles, *J. Appl. Meteorol.*, *38*, 607–616, doi:10.1175/1520-0450(1999)038<0607:EOSMOT>2.0.CO;2.
- Jacobson, M. Z. (2001a), GATOR-GCMM: A global through urban scale air pollution and weather forecast model. 1. Model design and treatment of subgrid soil, vegetation, roads, rooftops, water, sea ice, and snow, *J. Geophys. Res.*, *106*, 5385–5402, doi:10.1029/2000JD900560.
- Jacobson, M. Z. (2001b), GATOR-GCMM: 2. A study of day- and nighttime ozone layers aloft, ozone in national parks, and weather during the SARMAP field campaign, *J. Geophys. Res.*, *106*, 5403–5420, doi:10.1029/2000JD900559.
- Jacobson, M. Z. (2002), Analysis of aerosol interactions with numerical techniques for solving coagulation, nucleation, condensation, dissolution, and reversible chemistry among multiple size distributions, *J. Geophys. Res.*, *107*(D19), 4366, doi:10.1029/2001JD002044.
- Jacobson, M. Z. (2003), Development of mixed-phase clouds from multiple aerosol size distributions and the effect of the clouds on aerosol removal, *J. Geophys. Res.*, *108*(D8), 4245, doi:10.1029/2002JD002691.
- Jacobson, M. Z. (2006), Effects of absorption by soot inclusions within clouds and precipitation on global climate, *J. Phys. Chem.*, *110*, 6860–6873.
- Jacobson, M. Z. (2008), On the causal link between carbon dioxide and air pollution mortality, *Geophys. Res. Lett.*, *35*, L03809, doi:10.1029/2007GL031101.

- Jacobson, M. Z., and Y. J. Kaufman (2006), Wind reduction by aerosol particles, *Geophys. Res. Lett.*, *33*, L24814, doi:10.1029/2006GL027838.
- Jacobson, M. Z., Y. J. Kaufman, and Y. Rudich (2007), Examining feedbacks of aerosols to urban climate with a model that treats 3-D clouds with aerosol inclusions, *J. Geophys. Res.*, *112*, D24205, doi:10.1029/2007JD008922.
- Kahrl, W. L. (Ed.) (1979), *The California Water Atlas*, Gov. Off. of Plann. and Res., Sacramento, Calif.
- Ketefian, G. S., and M. Z. Jacobson (2009), A mass, energy, vorticity, and potential enstrophy conserving boundary treatment scheme for the shallow water equations, *J. Comput. Phys.*, *228*, 1–32, doi:10.1016/j.jcp.2008.08.009.
- Kueppers, L. M., M. A. Snyder, and L. C. Sloan (2007a), Irrigation cooling effect: Regional climate forcing by land-use change, *Geophys. Res. Lett.*, *34*, L03703, doi:10.1029/2006GL028679.
- Kueppers, L. M., et al. (2007b), Seasonal temperature responses to land use change in the western United States, *Global Planet. Change*, doi:10.1016/j.gloplacha.2007.03.005.
- Landsberg, J. J., D. B. B. Powell, and D. R. Butler (1973), Microclimate of an apple orchard, *J. Appl. Ecol.*, *10*, 881–896, doi:10.2307/2401878.
- Lanicci, J. M., T. N. Carlson, and T. T. Warner (1987), Sensitivity of the Great Plains severe-storm environment to soil-moisture distribution, *Mon. Weather Rev.*, *115*, 2660–2673, doi:10.1175/1520-0493(1987)115<2660:SOTGPS>2.0.CO;2.
- Lobell, D. B., G. Bala, and P. B. Duffy (2006), Biogeophysical impacts of cropland management changes on climate, *Geophys. Res. Lett.*, *33*, L06708, doi:10.1029/2005GL025492.
- Mahfouf, J.-F., E. Richard, and P. Mascart (1987), The influence of soil and vegetation on the development of mesoscale circulations, *J. Appl. Meteorol.*, *26*, 1483–1495, doi:10.1175/1520-0450(1987)026<1483:TIO SAV>2.0.CO;2.
- Marticorena, B., G. Bergametti, B. Aumont, Y. Callot, C. N'Doume, and M. Legrand (1997), Modeling the atmospheric dust cycle: 2. Simulation of Saharan dust sources, *J. Geophys. Res.*, *102*, 4387–4404, doi:10.1029/96JD02964.
- Martilli, A. (2002), Numerical study of urban impact on boundary layer structure: Sensitivity to wind speed, urban morphology, and rural soil moisture, *J. Appl. Meteorol.*, *41*, 1247–1266, doi:10.1175/1520-0450(2002)041<1247:NSOUIO>2.0.CO;2.
- Miller, D. A., and R. A. White (1998), A conterminus United States multi-layer soil characteristics data set for regional climate and hydrology modeling, *Earth Inter.*, *2*.
- Moore, N., and S. Rojstaczer (2001), Irrigation-induced rainfall and the Great Plains, *J. Appl. Meteorol.*, *40*, 1297–1309, doi:10.1175/1520-0450(2001)040<1297:II RATG>2.0.CO;2.
- Mortlock, A. M., and R. Van Alstyne (1998), Military, charter, unreported domestic traffic and general aviation: 1976, 1984, 1992, and 2015 emission scenarios, *NASA Rep.*, *CR-1998–207639*. (Available at [http://ntrs.nasa.gov/archive/nasa/casi.ntrs.nasa.gov/19980047346\\_1998120131.pdf](http://ntrs.nasa.gov/archive/nasa/casi.ntrs.nasa.gov/19980047346_1998120131.pdf))
- Ookouchi, Y., M. Segal, R. C. Kessler, and R. P. Pielke (1984), Evaluation of soil moisture effects on the generation and modification of mesoscale circulations, *Mon. Weather Rev.*, *112*, 2281–2292, doi:10.1175/1520-0493(1984)112<2281:EOSMEO>2.0.CO;2.
- Peet, S. D. (1907), In the Tulare Basin, *Am. Antiquarian*, *29*(1), 108.
- Salas, W., P. Green, S. Frolking, C. Li, and S. Boles (2006), Estimating irrigation water use for California agriculture: 1950s to present, *CEC-500–2006–057*, PIER Energy-Related Environ. Res., Calif. Energy Comm., Sacramento.
- Segal, M., Z. Pan, R. W. Turner, and E. S. Takle (1998), On the potential impact of irrigated areas in North America on summer rainfall caused by large-scale systems, *J. Appl. Meteorol.*, *37*, 325–331.
- Sutkus, D. J., S. L. Baughcum, and D. P. DuBois (2001), Scheduled civil aircraft emission inventories for 1999: Database development and analysis, *NASA Rep.*, *CR-2001–211216*. (Available at <http://gltrs.grc.nasa.gov/reports/2001/CR-2001-211216.pdf>)
- U.S. Environmental Protection Agency (USEPA) (2006a), Clearinghouse for inventories and emission factors, <http://www.epa.gov/ttn/chieff/>.
- U.S. Environmental Protection Agency (USEPA) (2006b), AIR data, <http://www.epa.gov/air/data/>.
- U.S. Geological Survey (USGS) (1999), 1-km resolution global landcover characteristics data base, derived from Advanced Very High Resolution Radiometer (AVHRR) data from the period April 1992 to March 1993, Sioux Falls, S. D.
- U.S. Geological Survey (USGS) (2008a), MODIS/Aqua Leaf-Area Index, <http://edcdaac.usgs.gov/modis/myd15a2v4.asp>.
- U.S. Geological Survey (USGS) (2008b), MODIS/Aqua albedo data, <http://edcdaac.usgs.gov/modis/mcd43c1v4.asp>.
- Western Regional Climate Center (2006), Western U.S. climate historical summaries, <http://www.wrcc.dri.edu/Climsum.html>.
- Zeng, X., R. E. Dickinson, A. Walker, M. Shaikh, R. S. DeFries, and J. Qi (2000), Derivation and evaluation of global 1-km fractional vegetation cover data for land modeling, *J. Appl. Meteorol.*, *39*, 826–839, doi:10.1175/1520-0450(2000)039<0826:DAEOGK>2.0.CO;2.
- Zhang, D., and R. A. Anthes (1982), A high-resolution model of the planetary boundary layer—Sensitivity tests and comparisons with SESAME-79 data, *J. Appl. Meteorol.*, *21*, 1594–1609, doi:10.1175/1520-0450(1982)021<1594:AHRMOT>2.0.CO;2.

---

M. Z. Jacobson, Department of Civil and Environmental Engineering, Stanford University, Stanford, CA 94305-4020, USA. ([jacobson@stanford.edu](mailto:jacobson@stanford.edu))